

Isothermal transformation of β phase in Cu-rich Cu–Al–Sn alloys

A. K. Chakrabarty^a, K. T. Jacob^b

^aWest Bengal University of Technology, Kolkata, India.

^bDepartment of Materials Engineering, Indian Institute of Science, Bangalore, India

Microstructural changes resulting from isothermal decomposition of the β -phase have been studied in Cu-rich binary Cu–Al and ternary Cu–Al–Sn alloys containing up to 3 at.% Sn at temperatures from 873 to 673 K. Results are presented as TTT diagrams. The decomposition occurs in several stages, each of which involves the establishment of metastable equilibrium between β and one or more of the product phases α , β_1 and γ_2 . Addition of Sn has been shown to increase the stability of the ordered β_1 -phase in relation to β . In alloys containing more than 2 at.% Sn, the β_1 emerges as a stable phase. At low Sn concentrations β_1 is metastable. An important new finding is the existence of three-phase equilibrium microstructure containing α , β_1 and γ_2 . Increasing addition of Sn alters the morphology of β_1 from rosettes to dendrites and finally to Widmanstätten needles.

Keywords: Microstructure; TTT diagram; Metastable equilibrium; Precipitate morphology; Three-phase equilibria

1. Introduction

Cu-rich alloys of the ternary system Cu–Al–Sn have several potential applications because of their abrasion and corrosion resistance. The abrasion resistance is attributed to the high hardness of the β -phase in the Cu–Al–Sn system. Smith and Lindief [1] applied the isothermal transformation technique of Davenport and Bain [2] to study the decomposition of high temperature β -phase with a disordered bcc structure in the binary system Cu–Al. They studied an alloy of near-eutectoid composition (24 at.% Al). The existence of a metastable ordered phase β_1 in the Cu–Al binary system near the Cu_3Al stoichiometric composition has been recognized by several investigators [1, 3–6]. Smith and Lindief [1] provided the first microstructural evidence of the rosette shaped ordered phase β_1 . Using a high temperature X-ray camera on a single crystal specimen of composition 25.5 at.% Al, Wassermann [4] showed that β_1 phase has an ordered bcc structure at 593 K after rapid cooling from 893 K. Rapid heating of β_1 resulted in the formation of β and it was suggested that the $\beta \rightleftharpoons \beta_1$ transformation is reversible. The rate of transformation of β to β_1 is very high compared with the formation of stable phases α and γ_2 by the eutectoid reaction. More β_1 formed with decreasing temperature; β transformed completely to β_1 below 698 K. Moon and Garwood [6] found it impossible to suppress the $\beta \rightarrow \beta_1$ reaction even at very high cooling rates.

In order to establish the effect of composition on the mode of transformation of β phase, Thomas [3] employed the isothermal transformation technique on four binary Cu–Al alloys containing 25.0, 24.3, 23.8 and 23.1 at.% Al. Separation of proeutectoid phases α and γ_2 was seen to disturb the metastable equilibrium between β and β_1 leading to one of the following binary metastable invariant reactions depending on alloy composition:

- (i) $\beta \leftrightarrow \alpha + \beta_1$ eutectoid reaction at 803 K, or
- (ii) $\beta + \gamma_2 \leftrightarrow \beta_1$ peritectoid reaction at 778 K,

Microstructurally the $\beta \leftrightarrow \alpha + \beta_1$ metastable eutectoid reaction is indicated by the formation of a layer of β_1 around α phase precipitating below 803 K. The metastable peritectoid reaction is revealed by the reversion of the matrix ($\beta + \beta_1$) to β in the region adjoining each proeutectoid γ_2 particle during isothermal transformation at temperatures above 778 K.

Prior to the work of Thomas [3] on metastable phases, Leach and Raynor [7] published their research on the constitution of Cu–Al–Sn alloys, with special reference to ternary compound formation. They identified a stable intermetallic phase of variable composition designated as T-phase. It exists between 778 and 1008 K and contains

75 (\pm 0.5) at.% Cu, with varying proportions of Al and Sn. The homogeneity region is widest at 793 K with Al varying between 8 and 23 at.% and Sn between 16.4 and 2 at.%. The T-phase was found to undergo ordering at temperatures below 778 K. The ordered phase was termed β' by Leach and Raynor [7], who determined isothermal ternary sections were at 923, 853, 845, 835, 819 and 778 K. T- phase has been shown to coexist with α , β and γ_2 . The T-phase has been redesigned as τ by Bochvar⁽⁸⁾ in a review of phase relations in the system Cu–Al–Sn.

The current research was undertaken to establish relationship between metastable β_1 of the Cu–Al binary system, and the ternary stable phase T (or τ). The influence of varying quantities of tin on the isothermal decomposition of β -phase is explored in this work.

2. Experimental procedure

2.1. Selection of alloys

Alloy compositions selected for study are listed in Table 1 and displayed on a ternary composition triangle in Fig. 1. They include three binary Cu–Al alloys, eutectoid (A), hypereutectoid (B) and hypoeutectoid (C), containing of 24, 25 and 23.5 at.% Al, respectively. Compositions of seven ternary alloys D, E, F, H, J, M and N are situated in the β stability field of the Cu–Al–Sn ternary isotherm at 923 K. Another five ternary alloys G, K, L, O and P are located between the stability domains of β and T phases.

2.2. Alloy preparation and analysis

Melting and alloying were carried out in a graphite crucible using a vacuum induction melting furnace. The charge consisted of electrolytic-grade copper, aluminum and tin of 99.95 % purity. Alloy ingots were hot pressed and then hot rolled to sheet of 1.5 mm thickness. Samples from the hot worked alloys were homogenized at 1073 K and then water quenched. Samples for chemical analysis were collected by drilling. The nominal and actual compositions are shown in Table 1. For the three binary alloys the compositions were also confirmed by microscopic analysis after annealing for \sim 260 ks at 843 K, just above the $\beta \leftrightarrow \alpha + \gamma_2$ eutectoid isotherm, and subsequent quenching in water. There was generally good agreement between the nominal compositions and the results of chemical analysis.

2.3. Isothermal transformation and metallographic analysis

The isothermal transformation technique of Davenport and Bain [2] was adopted. Samples approximately 1 cm square and 1.5 mm thick were heated to 1073(\pm 5) K to produce a

homogeneous β microstructure. The samples were directly quenched from 1073 K into either a molten salt (50:50 mixture of KNO_3 and NaNO_3) or molten lead maintained at selected temperatures. The samples were kept in the bath for isothermal transformation for predetermined periods of time. Temperature of the liquid bath was maintained by using a proportional controller and was measured by means of Pt/Pt-13%Rh thermocouple. The thermocouple was periodically checked against the freezing point of aluminum. The temperature gradient over a depth of 15 cm was less than 2 K, and at a given depth the temperature fluctuation was limited to ± 2 K. Finally the samples from salt / lead bath were quenched into an ice–water mixture. The samples were examined under an optical microscope after sectioning and metallographic preparation. Polished specimens were electrolytically etched using a 1 % aqueous solution of chromic acid as the electrolyte and aluminum as cathode. To estimate the relative amount of phases present in the microstructure, an image analyzing computer and point counting were adopted.

3. Results

The decomposition pattern in binary and ternary alloys can be best described by classifying the alloys into three groups. Group I consists of binary alloy C and ternary alloys D and H, in which α is the primary precipitate during isothermal decomposition.

Time–temperature–transformation (TTT) diagrams for these alloys are presented in Fig 2. In these diagrams different products and the kinetics of the reaction are shown as a function of temperature. Addition of Sn has a profound effect on the TTT diagram. For the binary alloy C, the sequence of changes involved in the decomposition of β -phase in the order of decreasing temperature can be summarized as follows:

- (a) $\beta \rightarrow$ proeutectoid α in β matrix
- (b) $\beta \rightarrow$ proeutectoid α in β matrix \rightarrow proeutectoid α in $(\alpha + \gamma_2)$
- (c) $\beta \rightarrow$ proeutectoid α surrounded by β_1 in β matrix \rightarrow proeutectoid α in $(\alpha + \gamma_2)$
- (d) $\beta \rightarrow \beta + \beta_1 \rightarrow$ proeutectoid α surrounded by β_1 in $(\beta + \beta_1)$ matrix \rightarrow proeutectoid α in $(\alpha + \gamma_2)$

These reactions often overlap resulting in a microstructure where β , β_1 , $(\alpha + \beta_1)$ and $(\alpha + \gamma_2)$ are all present together, for example at 773 K after 10^3 s.

Compared to the isothermal decomposition characteristics of binary alloy C, certain changes are observed for ternary alloys D and H. Prominent features are summarized in Table 2. The highest temperature at which β_1 separation occurs increases progressively from 788 K for alloy C, 793 K for alloy D, to 828 K for alloy H. Microstructural changes are presented in

Fig. 3. The morphology of the ordered phase changes from rosettes in the case of binary alloy C (Fig. 3a), dendrites in alloy D (Fig. 3b) to Widmanstätten needles in alloy H (Fig. 3c).

Etching contrast between β and β_1 increases with the lowering of transformation temperature. Figure 4a shows further microstructural evolution during isothermal transformation of binary alloy C. Globularization of the initial structure of metastable β_1 and disturbance caused by the precipitation of proeutectoid alpha are seen. The α needles are surrounded by β_1 below 798 K demonstrating the occurrence of the $\beta \leftrightarrow \alpha + \beta_1$ metastable eutectoid reaction. In the case of ternary alloy D below 813 K, the above metastable reaction is seen to occur directly in β phase (Fig. 4b). In alloy H, precipitation of α mainly occurs in the duplex structure $\beta + \beta_1$. Below 813 K, precipitation of α gives rise to an $\alpha + \beta_1$ microstructure as a result of the eutectoid reaction, as shown in Fig. 4c.

The transformation $\beta \leftrightarrow \alpha + \gamma_2$ does not occur in alloy H, as seen from the TTT diagram (Fig. 2c). Below 813 K, the equilibrium microstructure is $\alpha + \beta_1$. Between 828 and 818 K, prolonged heat treatment leads to the occurrence of a three-phase microstructure consisting of α , β and β_1 as shown in Fig. 5.

Group II alloys consist of binary alloy A of near eutectoid composition and ternary alloys E, J, M, and N, in which β_1 is the primary precipitate during isothermal decomposition of the β phase. TTT diagram for binary alloy A is shown in Fig. 6. The main features observed during isothermal decomposition of β -phase in this alloy in the order of decreasing transformation temperature can be summarized as follows:

- (a) $\beta \rightarrow \alpha + \gamma_2$
- (b) $\beta \rightarrow \beta + \beta_1 \rightarrow$ proeutectoid α surrounded by β_1 in $(\beta + \beta_1)$ matrix \rightarrow proeutectoid α surrounded by $(\alpha + \gamma_2)$
- (c) $\beta \rightarrow \beta_1 \rightarrow$ proeutectoid α in $\beta_1 \rightarrow$ proeutectoid α in $(\alpha + \gamma_2)$

As in the case of binary alloy C, β_1 -phase remains metastable and is precipitated as rosettes.

TTT diagrams for ternary alloys E and J are displayed in Fig. 7 and those for alloys M and N in Fig. 8. The effect of Sn additions can be seen from the TTT diagrams; significant features are summarized in Table 3. The highest temperature, at which β_1 separates from β , gradually increases from 798 to 863 K with increasing Sn addition. The morphology of β_1 changes from rosettes in the case of binary alloy A to dendrites in the case of alloys E and J and to Widmanstätten needles in the case of alloys M and N, similar to features observed in Fig. 4. β_1 also precipitates at grain boundaries and sub-boundaries of β in alloys M and N. This is demonstrated in Fig. 9 for alloy N. Addition of 1 at.% Sn results in lowering of the $\beta \leftrightarrow \alpha + \gamma_2$ eutectoid temperature. β_1 remains as a metastable phase in alloy E with 1 at.% Sn.

In the ternary alloys J, M and N with higher Sn content it emerges as a stable phase. The highest temperatures for β_1 separation for alloys J, M and N are higher than the maximum temperatures at which α separates (Figs. 7 and 8). As a result β_1 particles undergo substantial coarsening and spherodization with increased time of transformation as shown in Fig. 9 for alloy N. Separation of α from $(\beta + \beta_1)$ in alloys J, M and N results in microstructures exhibiting three-phase equilibrium $(\alpha + \beta + \beta_1)$ as seen in Fig. 10. Reduction in transformation temperature results in a reduced amount of β and increased amount of both α and β_1 , until below a certain temperature, the β -phase disappears as indicated in Table III. Below this temperature, α -phase that precipitates is surrounded by a β_1 envelope. In alloy J, prolonged holding at temperatures below 813 K results in a three-phase microstructure consisting of α , β_1 and γ_2 as shown in Fig. 11.

Group III consists of binary alloy B and ternary alloys F, G, K, L, O and P. It is convenient to subdivide these alloys into two subgroups:

- Group III(a): Alloys with total solute content of 25 at.%, i.e., alloys B, G, L and P.
- Group III(b): Alloys with total solute content of 24 at.%, i.e., alloys F, K and O.

Isothermal transformation diagrams of Group III(a) alloys are presented Figs. 12 and 13, and those of Group III(b) are presented in Fig. 14. Significant features are summarized in Table 4. Microstructural changes during isothermal decomposition of the ternary alloys G, L and P are very similar to that of binary alloy B. Alloys G and P are chosen as representatives of ternary alloys in this group to describe the microstructural changes shown in Figs. 15, 16 and 17.

The highest temperature at which β_1 separates directly from β could not be determined accurately because of the precipitation of a large number of proeutectoid γ_2 particles, which affect β/β_1 metastable equilibrium. There was evidence of a gradual rise in the maximum temperature at which β_1 separates with increasing Sn addition. The maximum temperature at which β is completely transformed to β_1 is also progressively raised by Sn addition (Table 4). β_1 appears as dendrites in 1 at.% Sn alloy and as Widmanstätten needles in alloys of higher Sn content, similar to features observed in Fig. 3. There is no microstructural evidence for the reaction $\beta \leftrightarrow \alpha + \gamma_2$ during isothermal decomposition in alloys with 2 and 3 at.% Sn. β_1 exists as a metastable phase in the 1 at.% Sn alloy and as a stable phase in alloys of higher Sn content.

In the binary hypereutectoid alloy, precipitation of γ_2 from a $(\beta + \beta_1)$ or β_1 matrix above the $\beta + \gamma_2 \rightarrow \beta_1$ peritectoid temperature results in the reversion of β_1 to β in regions adjoining γ_2 precipitates (Fig. 15a). The reversion reaction, $\beta_1 \rightarrow \beta + \gamma_2$, resembles a eutectoid reaction. In the ternary alloys, it is observed that above a certain temperature, precipitation of

γ_2 from either a ($\beta + \beta_1$) or β_1 matrix results in more extensive reversion (Figs. 15b, 16a and 16b). The product grows as an eutectoid like colony. Kinetics of growth is seen in Fig. 18. Just below this temperature, referred to as highest temperature for the peritectoid reaction (Table 4), precipitation of γ_2 from either ($\beta + \beta_1$) or β_1 matrix results in partial reversion of β_1 to β leading to three-phase equilibrium involving β , β_1 and γ_2 (Fig. 17). An increase in the transformation time within the peritectoid reaction zone results in coarsening of each of the three phases. On lowering the transformation temperature, the amount of β and γ_2 decreases (Fig. 17a and b), while that of β_1 increases until eventually the β phase disappears; the highest temperature at which this occurs is listed in Table 4. With increasing tin addition, the temperature range over which the peritectoid reaction occurs is increased (Table 4).

Prolonged transformation of β in the 2 at.% Sn alloy L at temperatures below 813 K results in the precipitation of α and three-phase equilibrium between α , β_1 and γ_2 , giving rise to a microstructure similar to that in Fig.11.

When γ_2 precipitates from β_1 matrix, dendrites of γ_2 are much smaller than when produced from β matrix. With increasing Sn additions, the γ_2 dendrites in β_1 matrix assume more complex form (Fig.19a). Increasing time of transformation results in simultaneous growth and coarsening. Eventually, most of the peripheral regions of γ_2 dendrites appear to form discontinuous shells (Fig.19b). After longer times, the individual spherical shells of γ_2 impinge on each other and form larger shells (19b).

Isothermal decomposition characteristics for Group III(b) alloys with 24 at.% solute content is similar to those of Group III(a) except for reduced volume fraction of γ_2 (Fig. 20). Kinetics of precipitation of γ_2 with time in the ternary alloy K with 2 at.% Sn was determined by quantitative metallography using both point counting technique and an image analyzer as shown in the Fig. 21. Volume percent of γ_2 increases with time. Difference in the amount of γ_2 between the two methods is around 2 %. Table 5 provides summary of significant observations.

Microstructures indicating three-phase equilibrium between α , β and β_1 are observed in the 3 at.% Sn alloy transformed at temperatures between 831 and 808 K. Prolonged transformation of 2 at.% Sn alloy (alloy K) below 813 K leads to the three-phase equilibrium between α , β_1 and γ_2 with features similar to those displayed in Fig.11.

4. Discussion

4.1. Effect of Sn addition on the stability of the ordered phase β_1

Isothermal transformation studies reveal that addition of $\text{Sn} \geq 2$ at.% leads to β_1 emerging as a stable phase in the Cu-rich corner of the system Cu–Al–Sn. This is reflected in the change in the topology of the TTT diagrams. Temperature of formation of the ordered phase β_1 is raised significantly with increase in Sn content. The emergence of β_1 as a stable phase has an influence on the following reactions:

- 1) $\beta \leftrightarrow \alpha + \beta_1$
- 2) $\beta + \gamma_2 \leftrightarrow \beta_1$

The metastable reactions of the Cu–Al binary system become stable beyond 2 at.% Sn in Cu-rich Cu–Al–Sn alloys. This eventually results in a three-phase microstructure involving α , β and β_1 in the ternary alloys with $\text{Sn} \geq 2$ at.% and total solute content < 23.5 at.%. Evidence for occurrence of the reaction $\beta \leftrightarrow \alpha + \beta_1$ in the alloys of abovementioned composition is provided by the increase in both α and β_1 and decrease in β with progressive lowering of the transformation temperature. This ultimately results in the disappearance of β with lowering of temperature below 813 K; the microstructure completely transforms to α and β_1 .

In the ternary alloys with solute concentration > 23.5 at.% and $\text{Sn} \geq 2$ at.% Sn, the $\beta + \gamma_2 \leftrightarrow \beta_1$ peritectoid reaction gives rise to a stable three-phase microstructure consisting of β , β_1 and γ_2 phases. The existence of the peritectoid reaction is evidenced by the reduction in β and γ_2 phases with the lowering of transformation temperature, eventually leading to the disappearance of β -phase below 813 K.

The eutectoid reaction ($\beta \leftrightarrow \alpha + \gamma_2$) isotherm is progressively reduced with increasing Sn addition. Further, the reaction gets significantly retarded as seen from the TTT diagrams with progressively higher additions of Sn. This is illustrated in Fig. 22, in which volume of eutectoid has been plotted with respect to time of transformation for binary hypereutectoid alloy B and ternary hypereutectoid alloy G with 1 at.% Sn addition. In the ternary alloys J, K and L, each containing 2 at.% Sn, a three-phase equilibrium structure consisting of α , β_1 and γ_2 is seen to develop below 813 K (Fig. 11). In a subsequent paper, which will deal with the ternary isothermal sections and experiments on eight additional ternary alloys, it will be shown that such microstructure has developed due to the occurrence of a ternary invariant reaction $\beta + \gamma_2 \leftrightarrow \alpha + \beta_1$. The mechanism by which Sn addition increases stability of the ordered phase β_1 will also be described in this paper, where a unified understanding of the effect of different third elements such as Al, Ga, Zn, Mn, Sn and In will be presented.

4.2. Effect of Sn on the morphology of β_1

It is observed in the present work that the nucleation of β_1 in β is very rapid during isothermal transformation. β_1 separates as rosettes in binary alloys, but there is a tendency to dendrite morphology in the hypereutectoid alloys. It forms as dendrites in ternary alloys with 1 at.% Sn. In alloys with 2 at.% Sn, β_1 separates as dendrites at lower Al and as needles at higher Al content. It separates only as needles in alloys containing 3 at.% Sn. In both the binary and ternary alloys, prolonged isothermal treatment results in spherodization of β_1 particles in order to reduce the total energy of the interphase boundaries.

Although the initial morphology of β_1 is the result of complex interplay of several factors, it can be rationalized in terms of the variation of elastic anisotropy of β_1 and elastic strain between crystals of β and β_1 with increasing Al in binary alloys and Sn in ternary alloys. Wassermann's [4] high temperature X-ray diffraction studies have indicated that Al occupies $\frac{1}{4} \frac{1}{4} \frac{1}{4}$, $\frac{1}{4} \frac{3}{4} \frac{3}{4}$, $\frac{3}{4} \frac{1}{4} \frac{3}{4}$, $\frac{3}{4} \frac{3}{4} \frac{1}{4}$ positions in the ordered DO_3 crystal structure of β_1 phase. Leach and Raynor [7] have demonstrated by high-temperature X-ray diffraction that the structure of their ternary β' phase (designated as β_1 in this study) in Cu-Al-Sn system is essentially the same as that identified by Wassermann. The structure can be visualized as the stacking together of eight body-centered unit cubes with Sn as the central atom. Because of the preferred positions of Al and Sn atoms in the ordered structure, elastic anisotropy will increase with Al and Sn concentration of β_1 .

Because of the higher atomic size of Al and Sn compared to Cu, unit cell dimensions of both β and β_1 increase with alloying addition. The ordering process is associated with a small volume contraction. Moreover, there is a difference in the composition of β and β_1 phases and this difference is temperature dependent. Electron probe micro analysis (EPMA) conducted on isothermally transformed ternary alloy M at 855 K during the present study have shown that β_1 contains twice the concentration of Sn as compared to the β phase. A full understanding of the β_1 morphology must await atomic scale modeling and experimental characterization of the β/β_1 interface using complementary techniques such as high resolution scanning transmission electron microscopy (STEM) and atom probe tomography.

4.3. Effect of Sn addition on morphology of γ_2

In the binary hypereutectoid alloys γ_2 separates from β in the form of dendrites. This orientation dependent growth can be explained by the "ledge mechanism" proposed by Aaronson et al. [9], assuming the existence of an initially immobile dislocation interface.

During prolonged transformation the initially semi-coherent interface becomes incoherent and hence is no longer immobile. Growth of γ_2 particles in a more isotropic manner with prolonged isothermal transformation is therefore expected.

Increasing under-cooling in this alloy result in faster growth of the individual dendritic branches. This conforms with Horvay and Cahn's [10] analysis. The outer boundary of γ_2 dendrites in the β_1 matrix has spherical shape. Each of the individual spherodized dendrites of γ_2 appear to join with adjacent dendrites, probably driven by reduction of surface energy.

5. Conclusions

Addition of Sn to Cu-Al alloys progressively changes the morphology of the ordered phase β_1 from rosettes to dendrites and further to Widmanstätten needles. An important conclusion drawn from both microstructure and TTT diagrams is the emergence of β_1 as a stable phase in Cu-rich alloys of the ternary Cu-Al-Sn when Sn concentration ≥ 2 at.%. The eutectoid reaction $\beta \leftrightarrow \alpha + \beta_1$ and peritectoid reaction $\beta + \gamma_2 \leftrightarrow \beta_1$, which are metastable in the binary Cu-Al system, become stable in ternary alloys for Sn ≥ 2 at.%. Below 813 K ($\alpha + \beta_1 + \gamma_2$) emerges as a three-phase field.

The eutectoid reaction, $\beta \leftrightarrow \alpha + \gamma_2$, is retarded by addition of Sn ≥ 1 at.%. The eutectoid temperature also is lowered by progressive Sn addition. The eutectoid reaction does not occur in ternary alloys with more than 1 at.% Sn.

The authors are grateful to late Dr. D. L. Thomas for provision of experimental facilities and guidance at the Department of Materials, Imperial College, London.

Correspondence Address

Professor K. T. Jacob

Department of Materials Engineering

Indian Institute of Science

Bangalore 560012

India.

Phone: +91 80 2293 2494

Fax: +91 80 2360 0472

E-mail: katob@materials.iisc.ernet.in

References

- [1] C.S. Smith, W.E. Lindief: Trans. AIME 104 (1933) 69.
- [2] E.S. Davenport, E.C. Bain: Trans. AIME, 90 (1930) 117.
- [3] D.L. Thomas: J. Inst. Metals, London 94 (1966) 250.
- [4] G.Wassermann: Metalwirtschaft 13 (1934) 133.
- [5] D.R.F. West, D.L. Thomas: J. Inst. Metals, London 83 (1955) 505.
- [6] J.R. Moon, R.D. Garwood: J. Inst. Metals, London 96 (1968) 17.
- [7] J.S.L. Leach, G.V. Raynor: Proc. Roy. Soc. London 224 (1954) 251.
- [8] N.R.Bochvar : in G. Petzow , G. Effenburg (Eds): Ternary Alloys – A Comprehensive Compendium of Evaluated Constitutional Data and Phase Diagrams, 1992, vol. 5, p.23, VCH Verlagsgesellschaft, Weinheim, FRG.
- [9] C. Laird, H.I. Aaronson: Acta Metall. 4 (1969) 505.
- [10] G. Horvay, J.W. Cahn: Acta Metall. 9 (1961) 695.

Figure Captions

- Fig. 1 Composition of alloys selected for study displayed on ternary triangle in relation to the stability domains of the β and T phases in the system Cu–Al–Sn.
- Fig. 2 TTT diagrams of (a) binary hypereutectoid alloy C, (b) ternary alloy D, and (c) ternary alloy H. The primary precipitate in all these alloys is α .
- Fig. 3 Effect of Sn addition on the morphology of β_1 phase: (a) formation of rosettes in binary alloys A and C, (b) formation of dendrites in binary alloy B and ternary alloys G, H, J and K, (c) formation of Widmanstätten needles in binary alloy L and ternary alloys M, N, O and P.
- Fig. 4 Evidence of $\beta \leftrightarrow \alpha + \beta_1$ eutectoid reaction: proeutectoid α surrounded by β_1 witnessed in binary and ternary alloys in which α is the primary precipitate.
- Fig. 5 Three-phase equilibrium microstructure of α (light), β (brown) and β_1 (pale) observed in the ternary alloy H.
- Fig. 6 TTT diagram for alloy A.
- Fig. 7 TTT diagrams for (a) alloy E and (b) alloy J.
- Fig. 8 TTT diagrams for (a) alloy M and (b) alloy N.
- Fig. 9 Effect of time of transformation on partial spherodization and coarsening in alloy N. (a) Coarsened needles and sub-boundary networks of β_1 in β matrix. (b) Nearly spherodized β_1 in β matrix, which shows martensitic structure formed during quenching from isothermal bath into water.
- Fig. 10 Three-phase microstructure of alloy N held at transformation temperature of 833 K for 10^6 s; α (light), β (brown) and β_1 (pale).
- Fig. 11 Three-phase microstructure of α (light, needle-shaped), β_1 (slightly darker than α) and γ_2 (blue tint) observed in ternary alloy J isothermally transformed at 793 K. Similar microstructure is also seen in alloys K and L after prolonged heat treatment below 813 K.
- Fig. 12 TTT diagram for binary and ternary hypereutectoid alloys containing 25 at.% total solute concentration; (a) alloy B, (b) alloy G.
- Fig. 13 TTT diagram for ternary hypereutectoid alloys containing 25 at.% total solute concentration; (a) alloy L, (b) alloy P.
- Fig. 14 TTT diagram for ternary hypereutectoid alloys containing 24 at.% total solute concentration: (a) alloy F, (b) alloy K, (c) alloy O.
- Fig. 15 Effect of Sn addition on reversion of β_1 to β around γ_2 precipitates in binary

and ternary hypereutectoid alloys: γ_2 (blue), reverted β (brown) in β_1 or ($\beta + \beta_1$) matrix; (a) alloy B, 798 K, 10^2 s, (b) alloy G, 798 K, 10^2 s.

Fig.16 Effect of Sn addition on reversion of β_1 to β around γ_2 precipitates in ternary alloy P: (a) 833 K, 10^3 s, (b) 833 K, 10^4 s.

Fig.17 Three-phase equilibrium microstructure in alloy P consisting of β (brown), β_1 (yellow) and γ_2 (blue) at (a) 831 K, 10^6 s, and (b) 823 K, 10^5 s.

Fig.18 Effect of Sn addition on kinetics of the $\beta_1 \leftrightarrow \beta + \gamma_2$ eutectoid reaction / transformation.

Fig.19 Morphology of γ_2 in β_1 matrix of alloy P: (a) dendrites of γ_2 in β_1 , present partly as small discontinuous rings, (b) growth, spherodization and impingement of γ_2 dendrites.

Fig. 20 Three-phase microstructure of alloy O consisting of β (brown), β_1 (yellow) and γ_2 (blue tint).

Fig. 21 Comparison of results of determination of volume of γ_2 in β matrix by means of (a) point counting and (b) image analyzing computer.

Fig. 22 Effect of ternary Sn addition on kinetics of $\beta \rightarrow \alpha + \gamma_2$ eutectoid reaction.

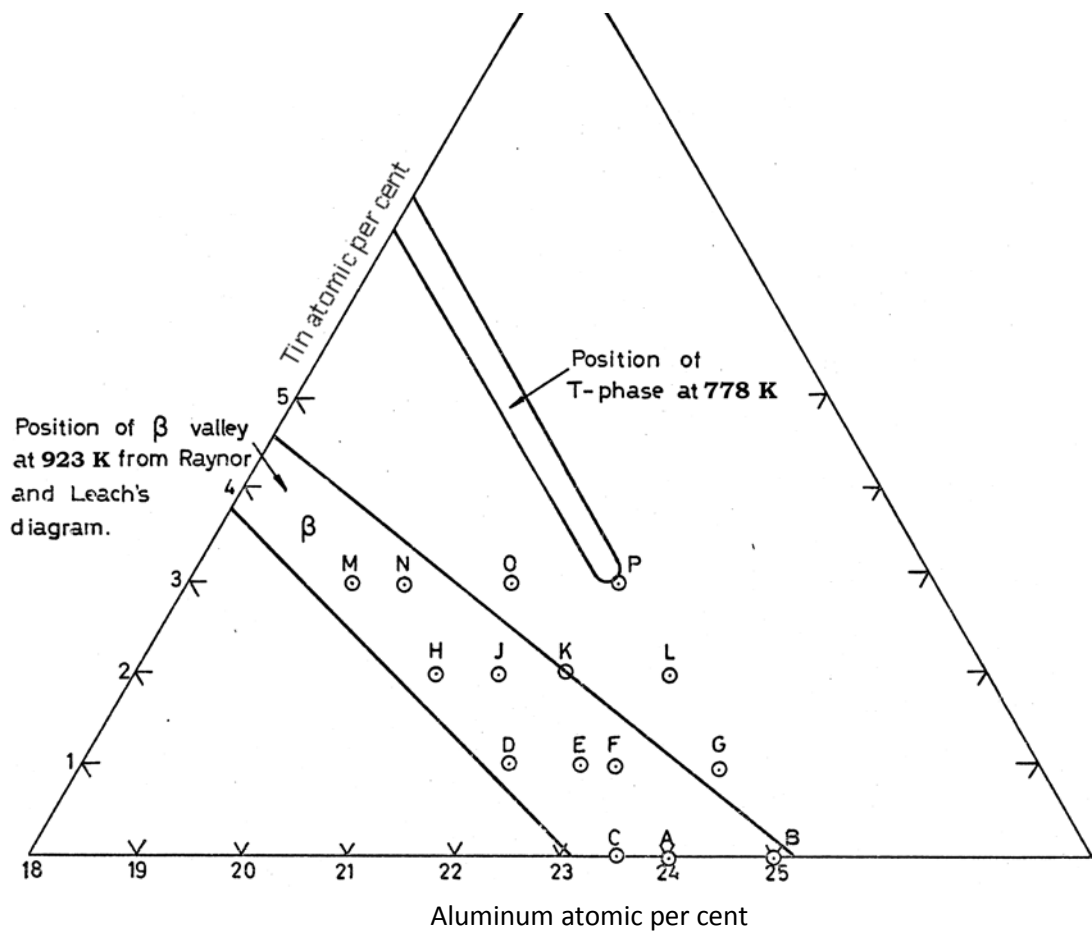


Fig. 1

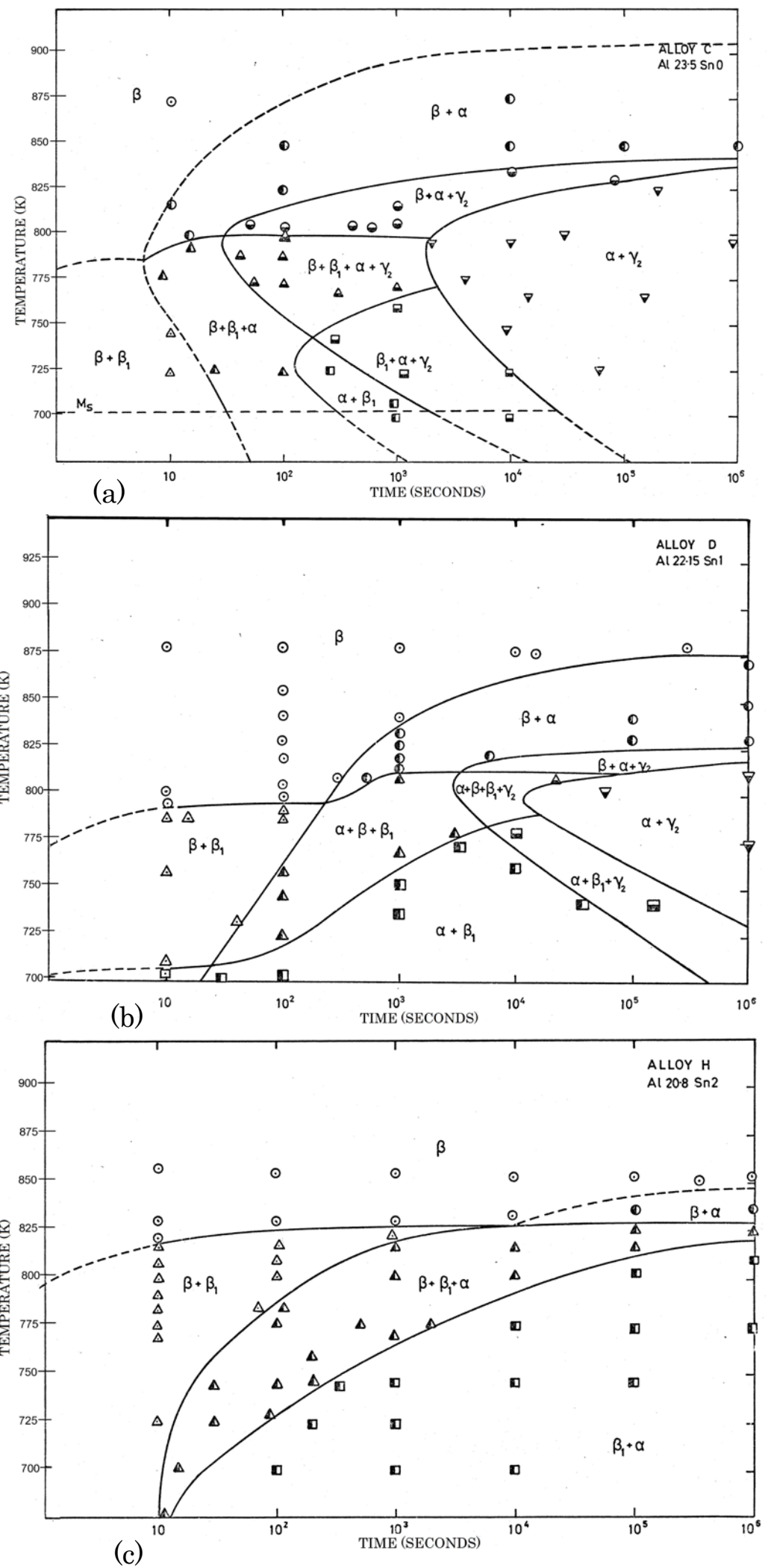
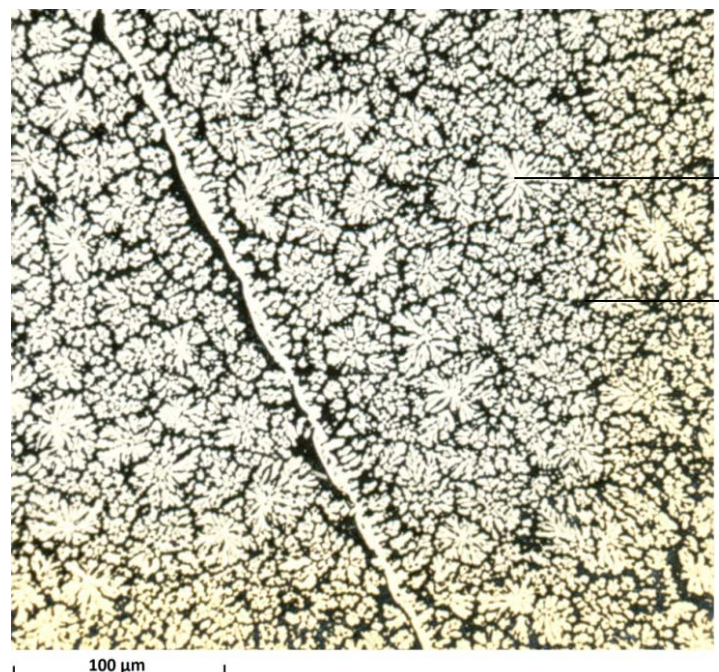
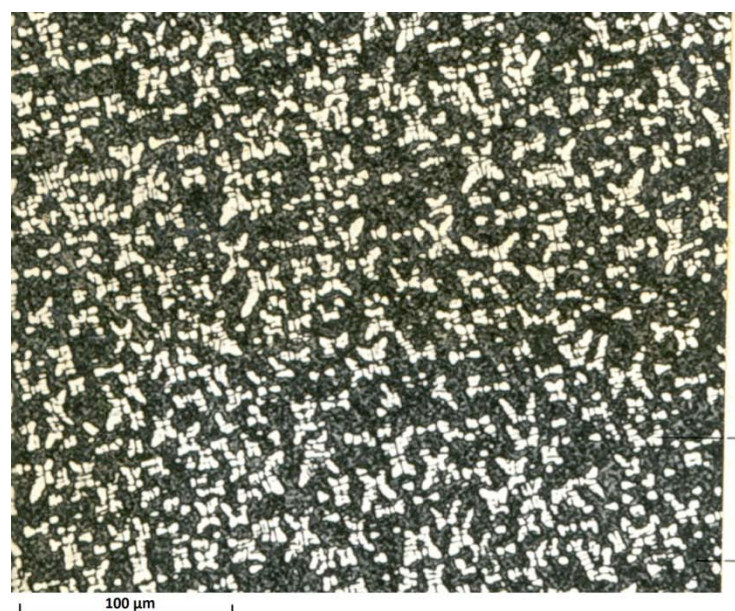


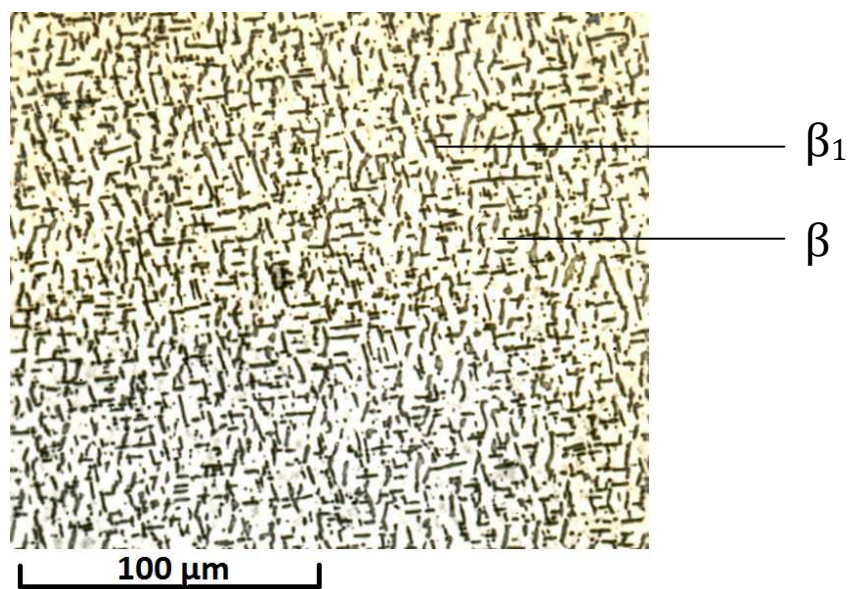
Fig. 2



(a)



(b)



(c)

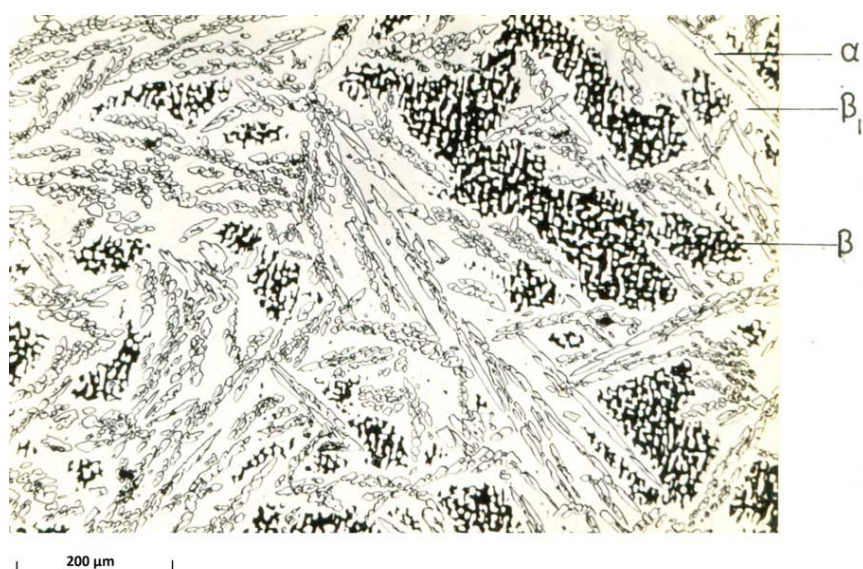
Fig. 3



(a)



(b)



(c)

Fig. 4

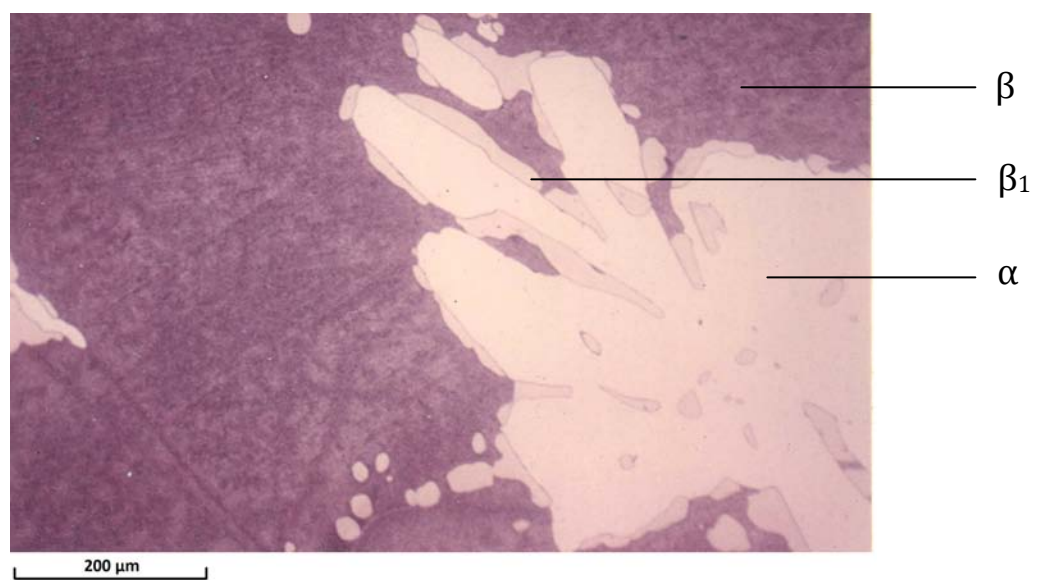


Fig. 5

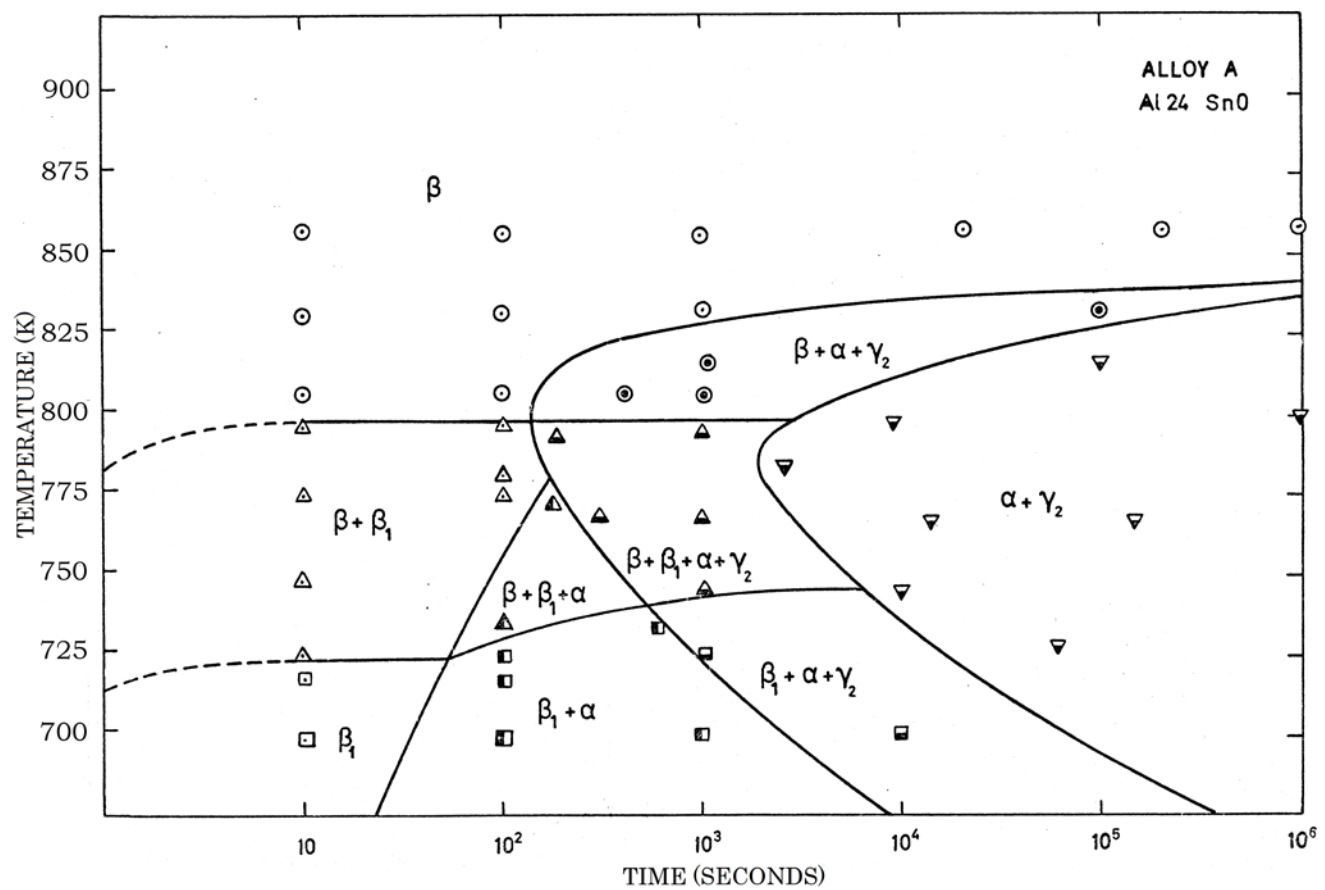


Fig. 6

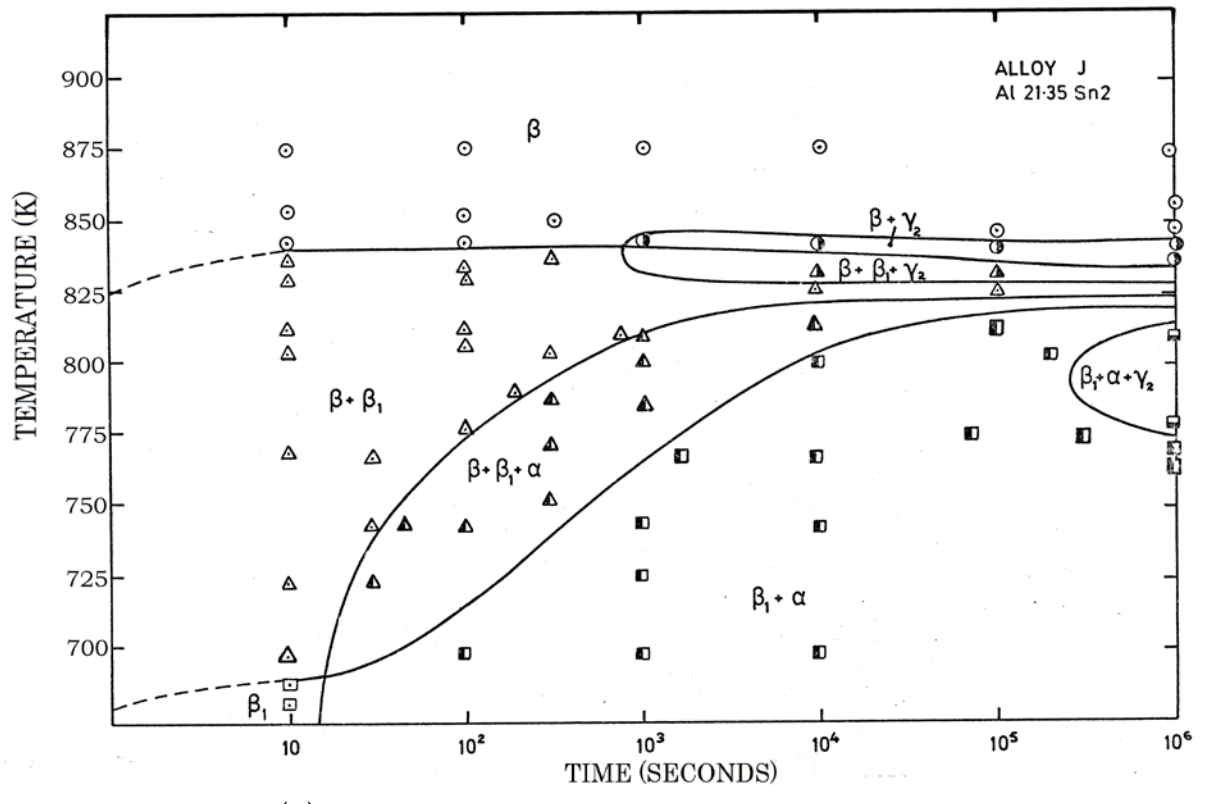
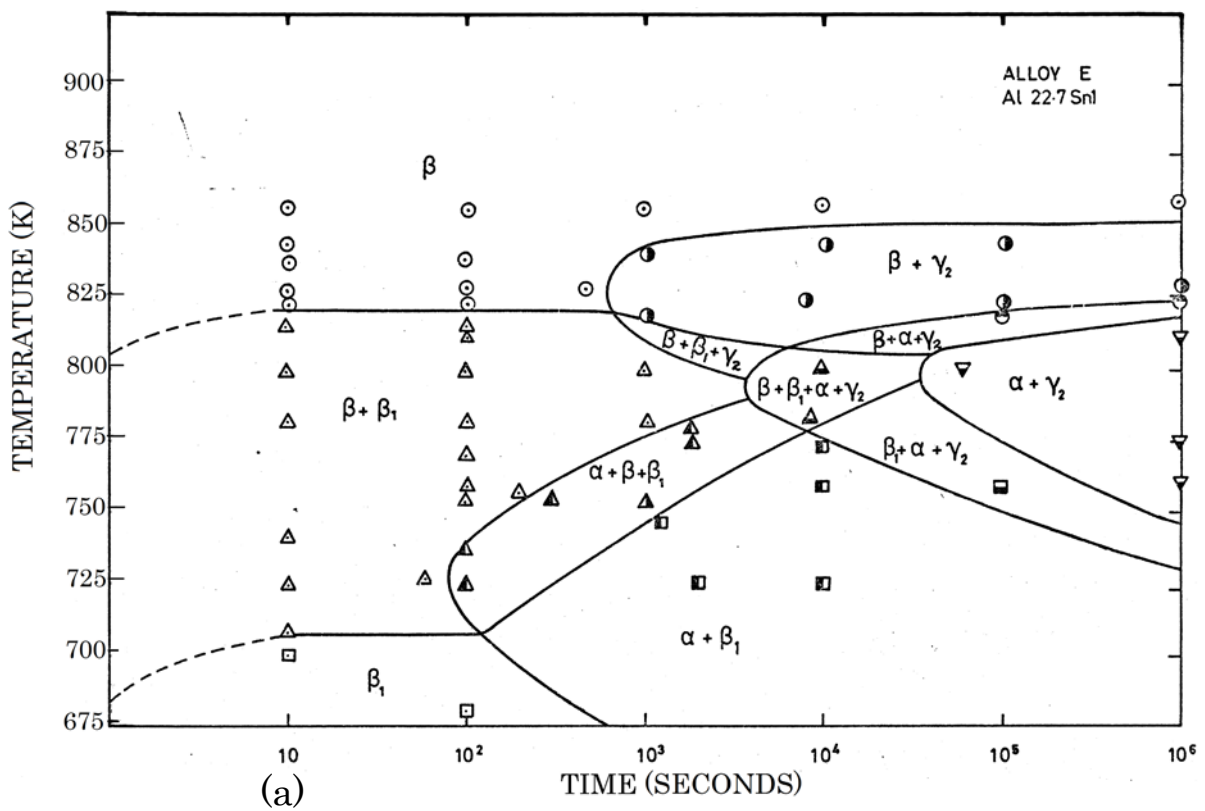
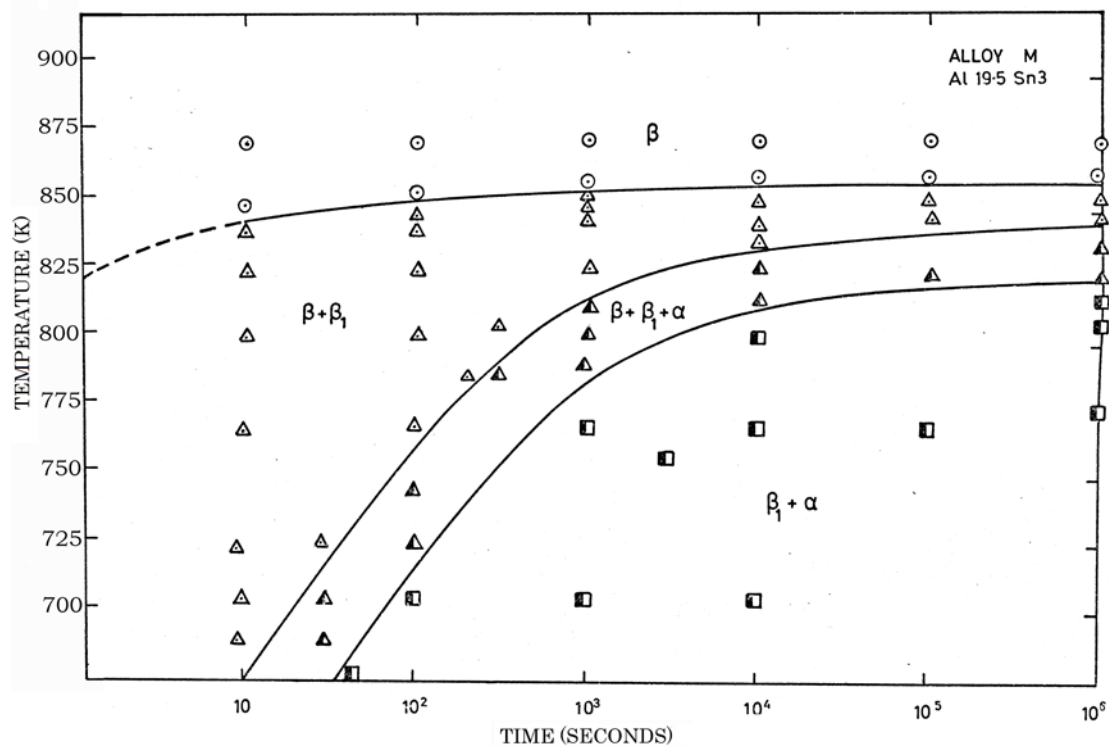
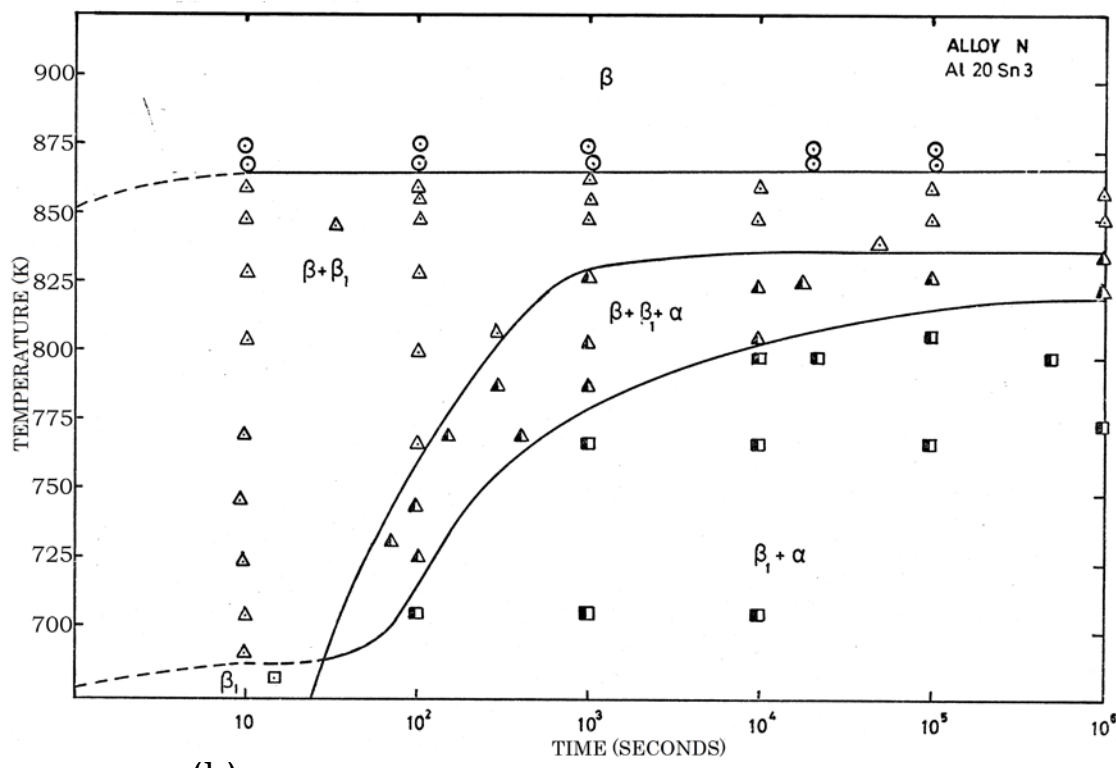


Fig. 7

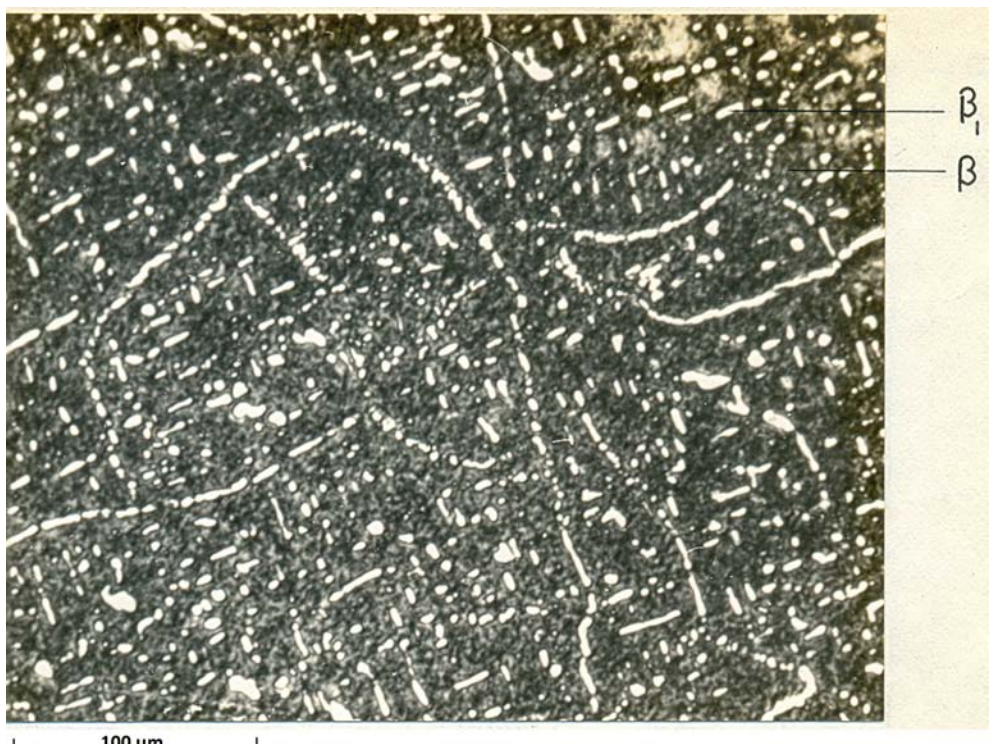


(a)

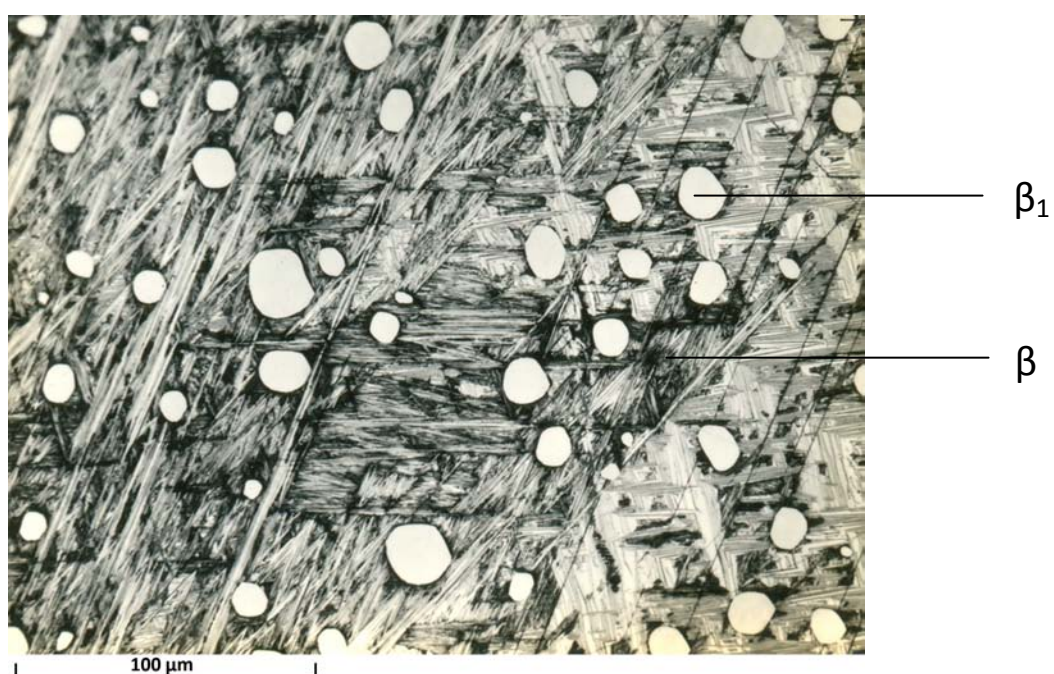


(b)

Fig. 8



(a)



(b)

Fig. 9

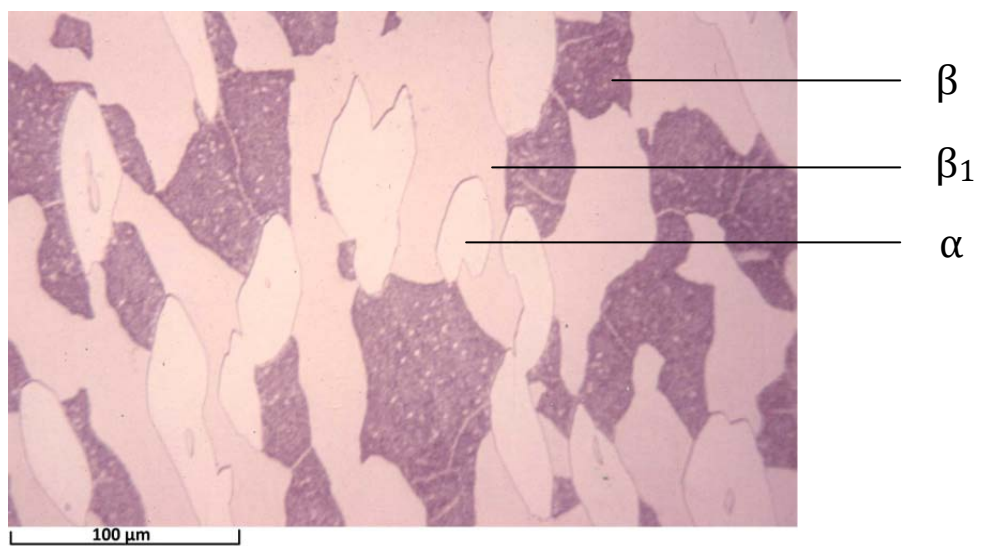


Fig. 10

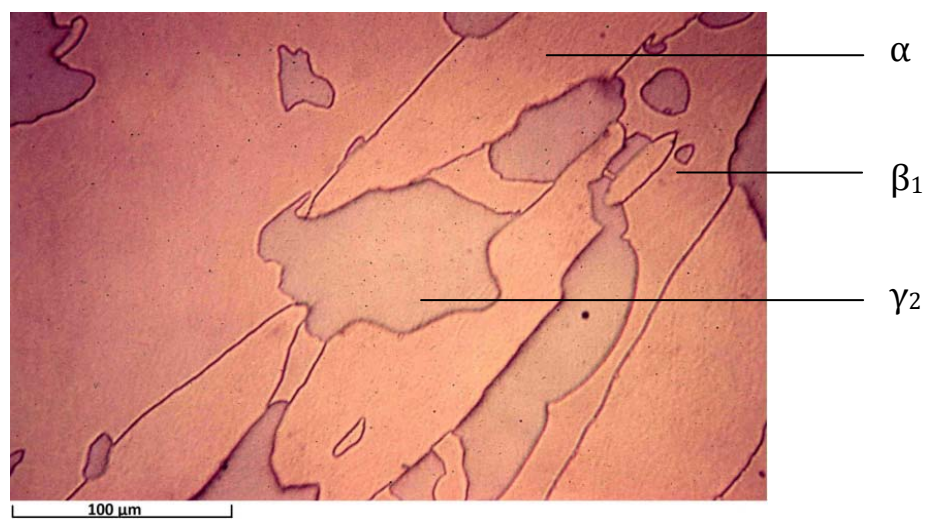


Fig. 11

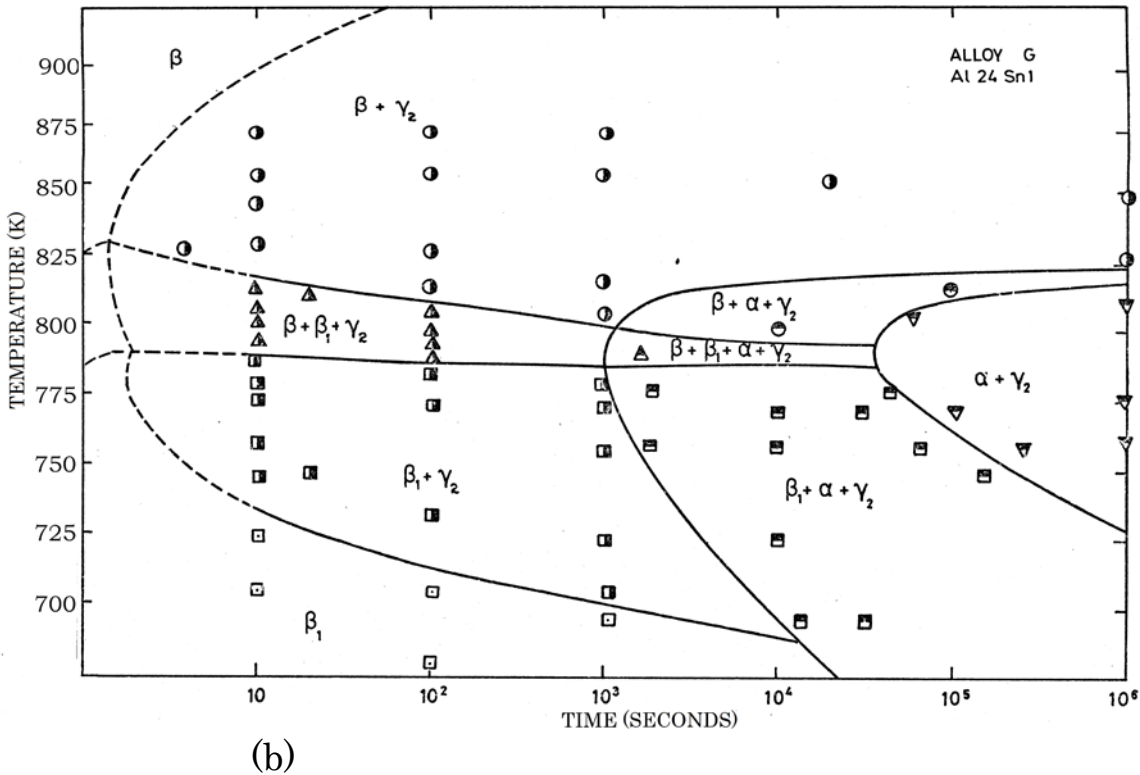
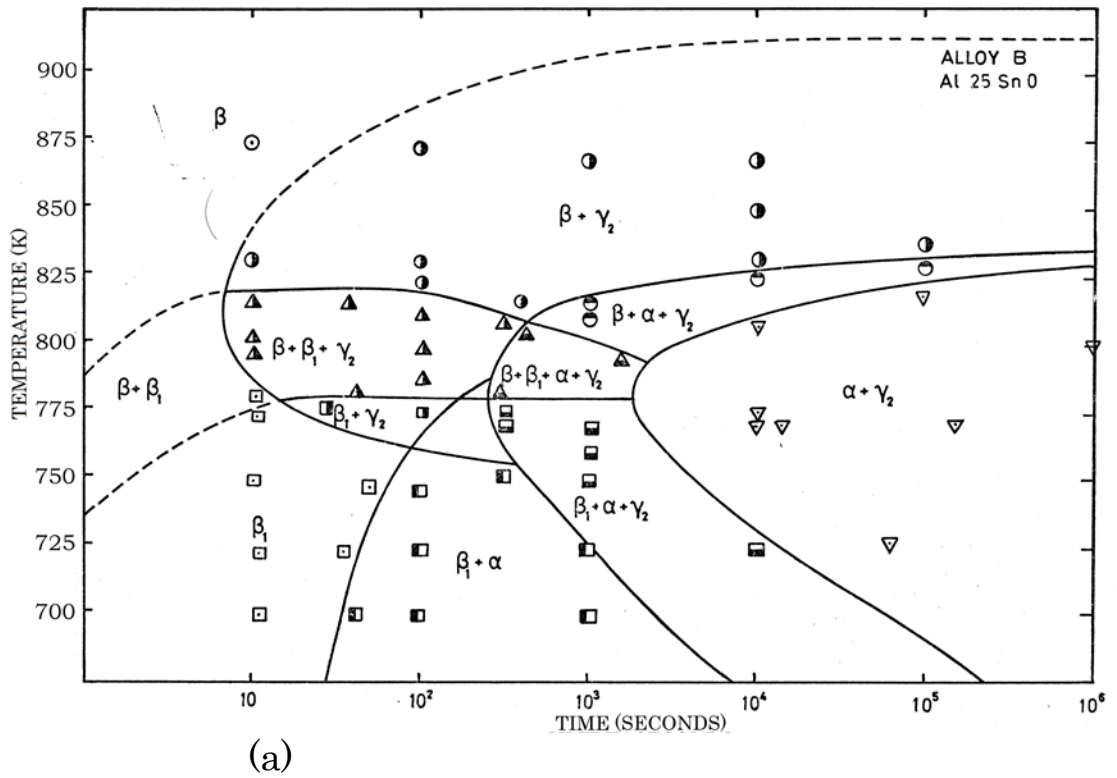
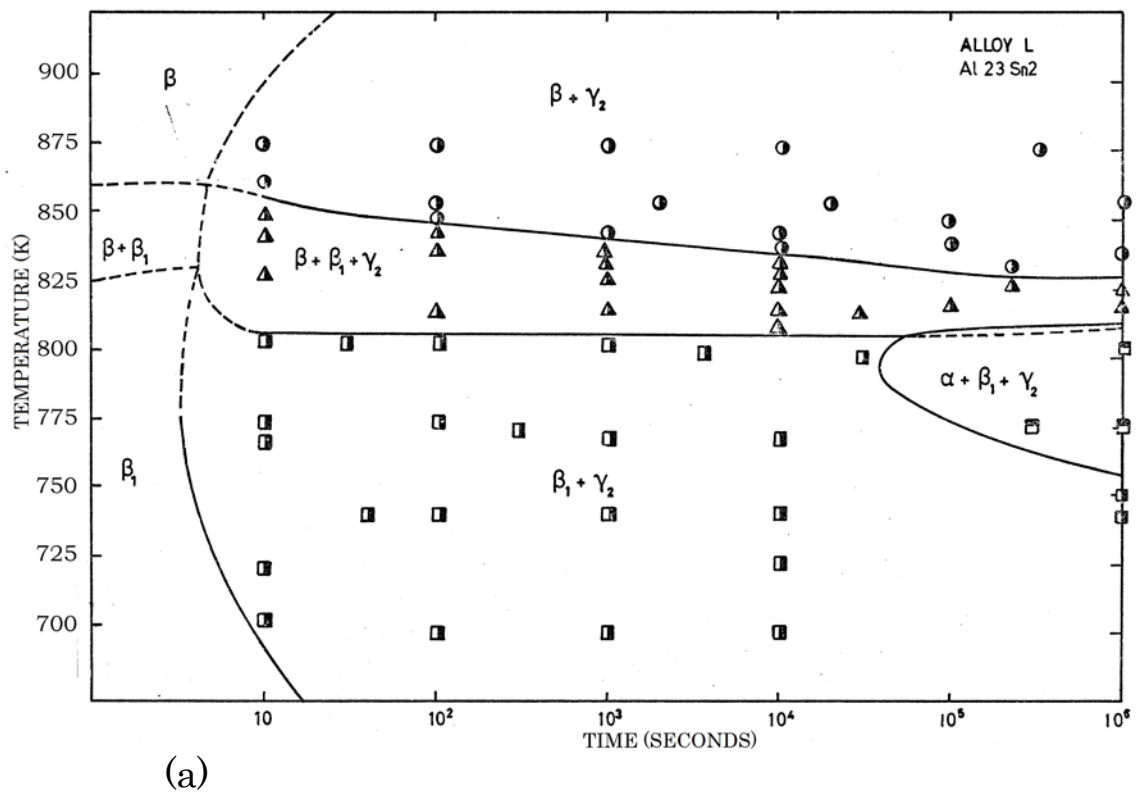
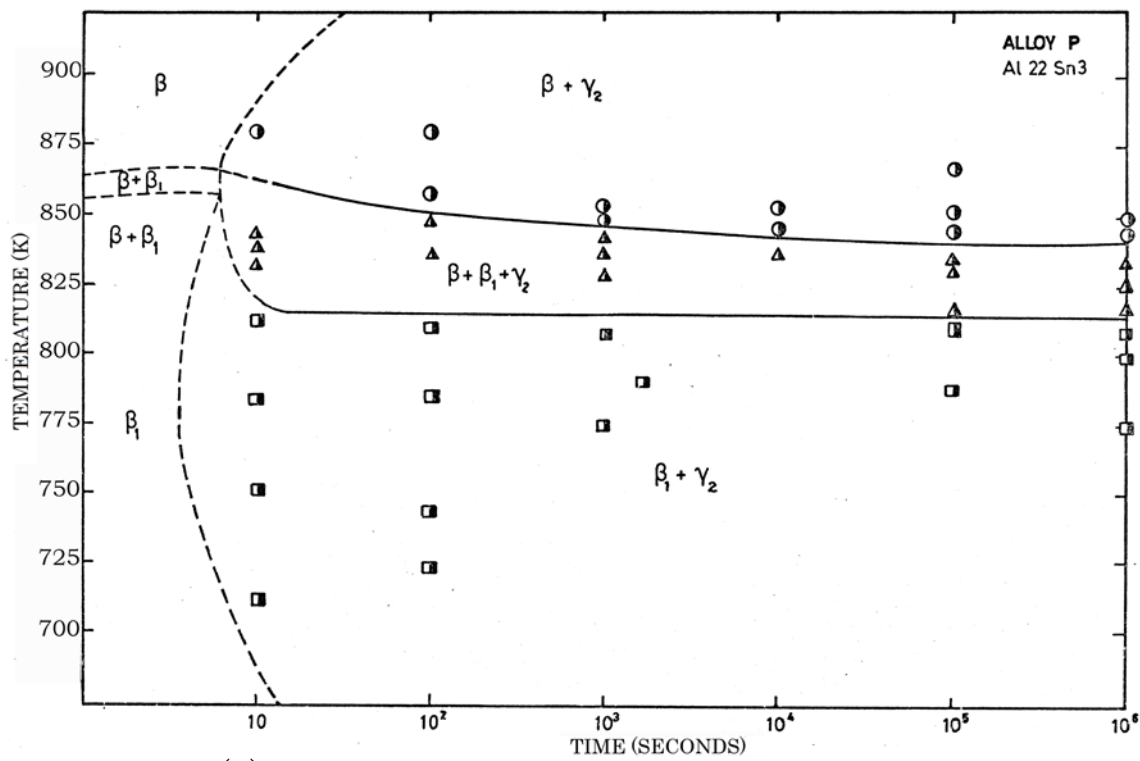


Fig. 12

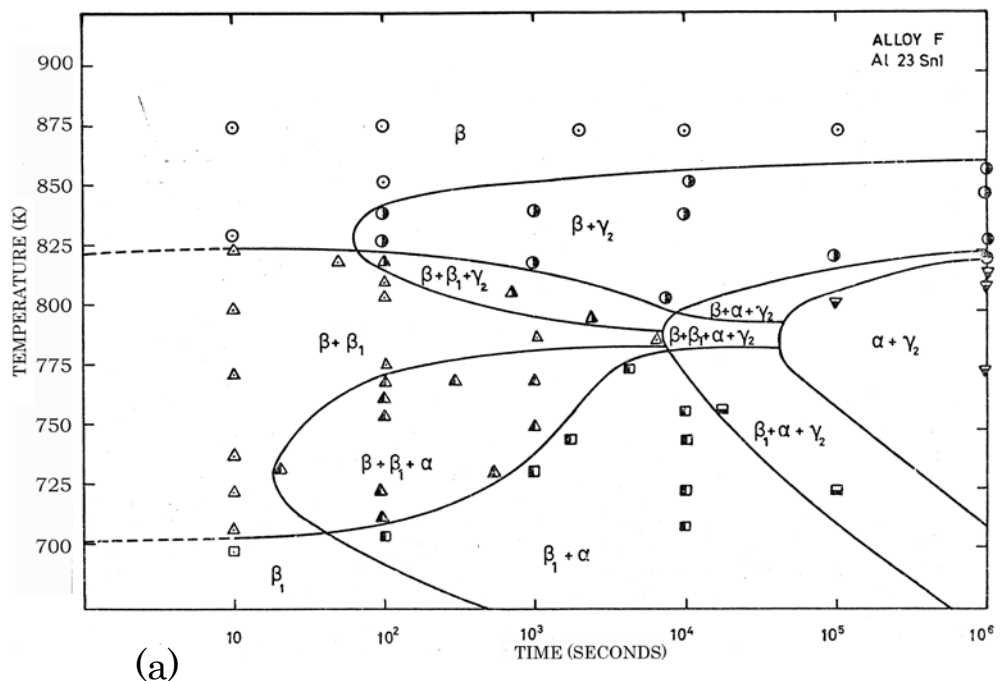


(a)

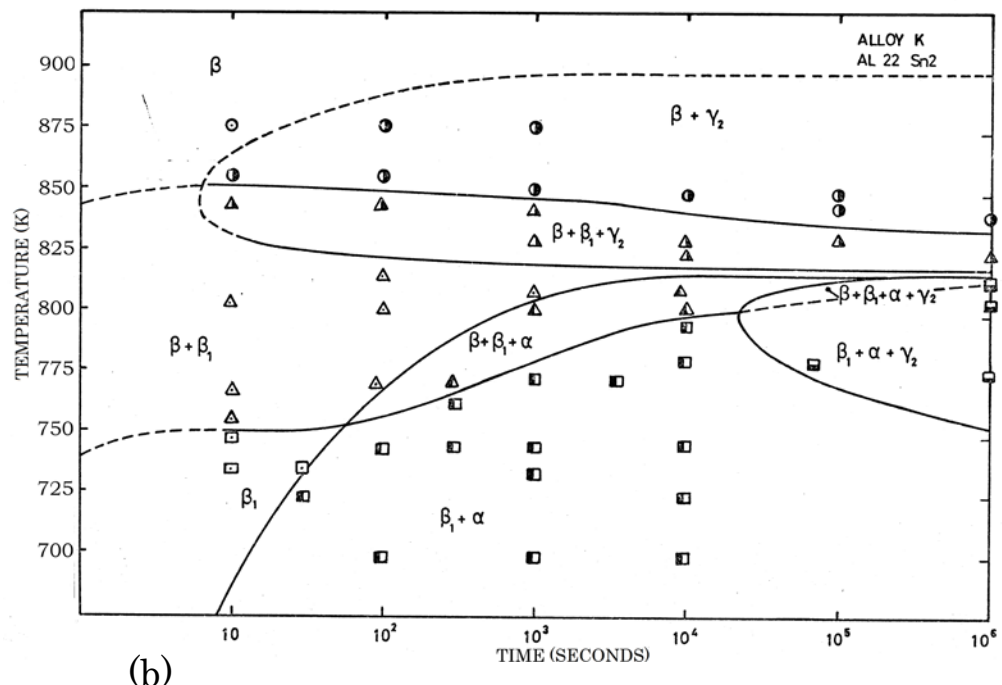


(b)

Fig. 13



(a)



(b)

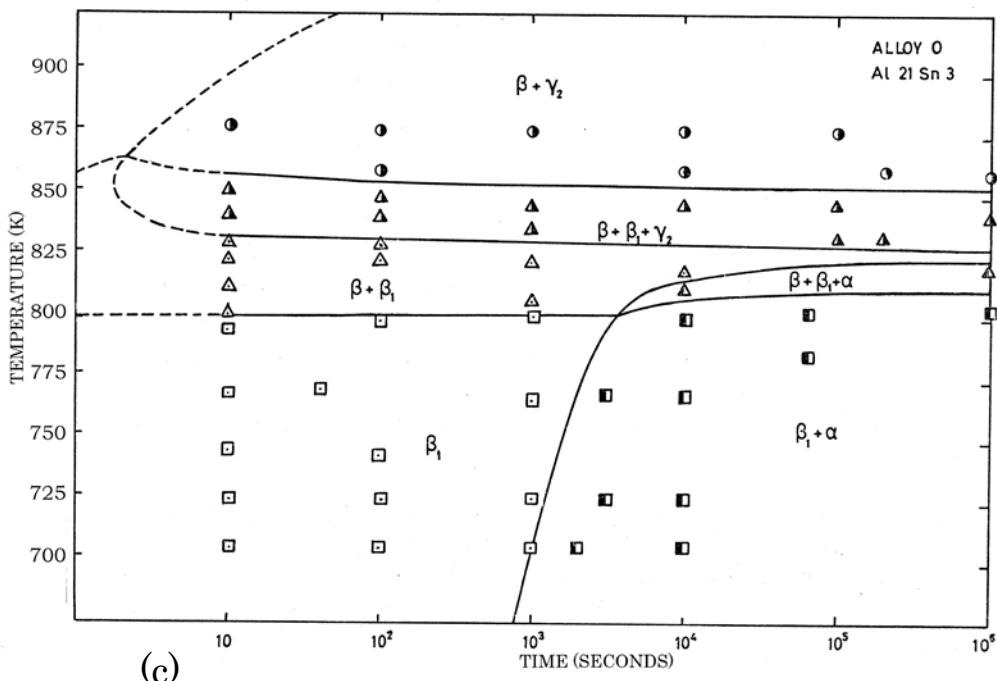
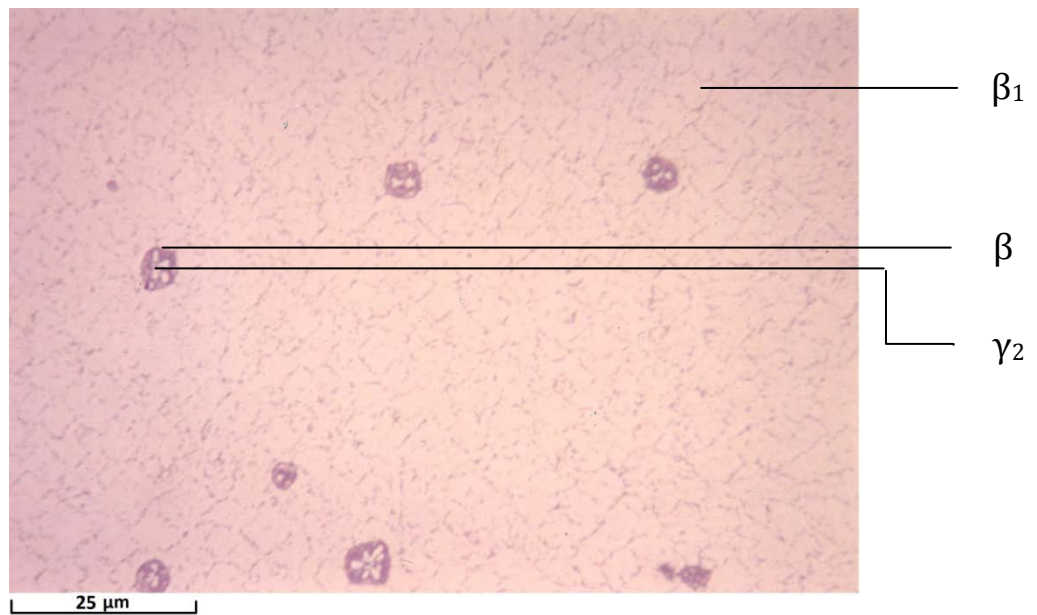
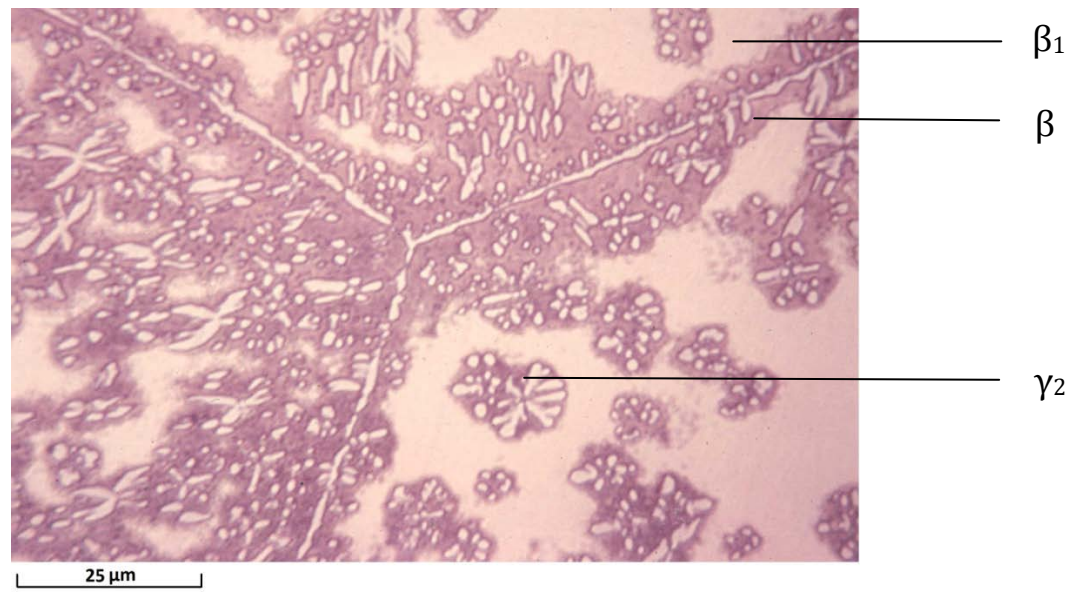


Fig. 14

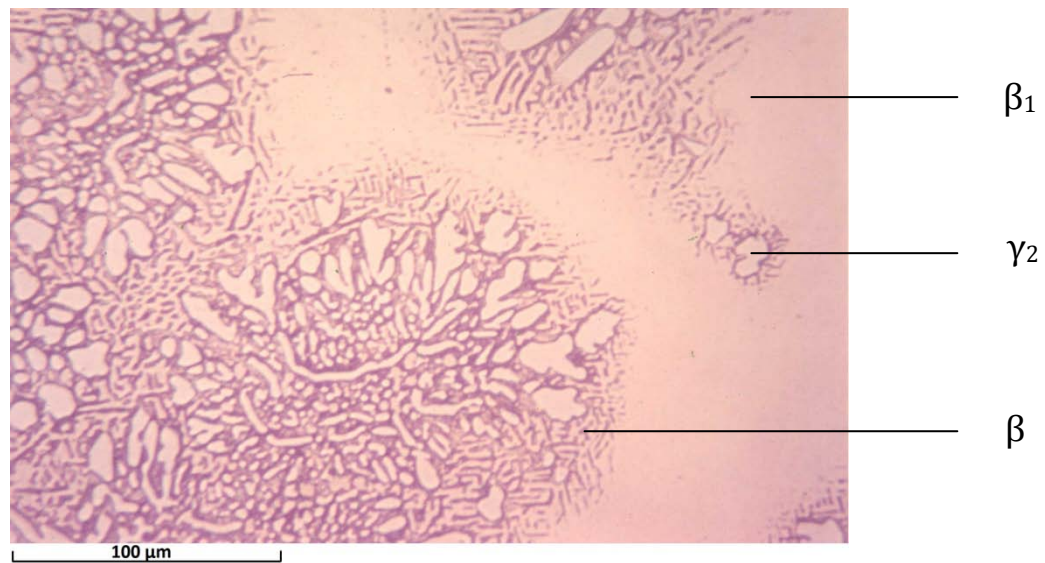


(a)

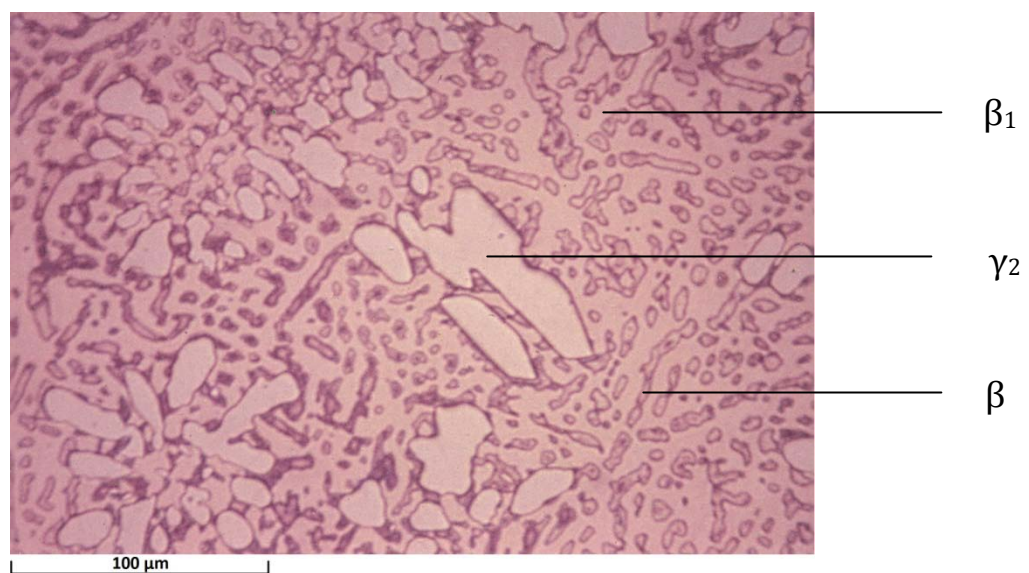


(b)

Fig. 15



(a)



(b)

Fig. 16

Curve 1 Alloy P (22 at.% Al 3 at.% Sn) 848 K
Curve 2 Alloy L (23 at.% Al 2 at.% Sn) 843 K
Curve 3 Alloy G (24 at.% Al 1 at.% Sn) 800 K

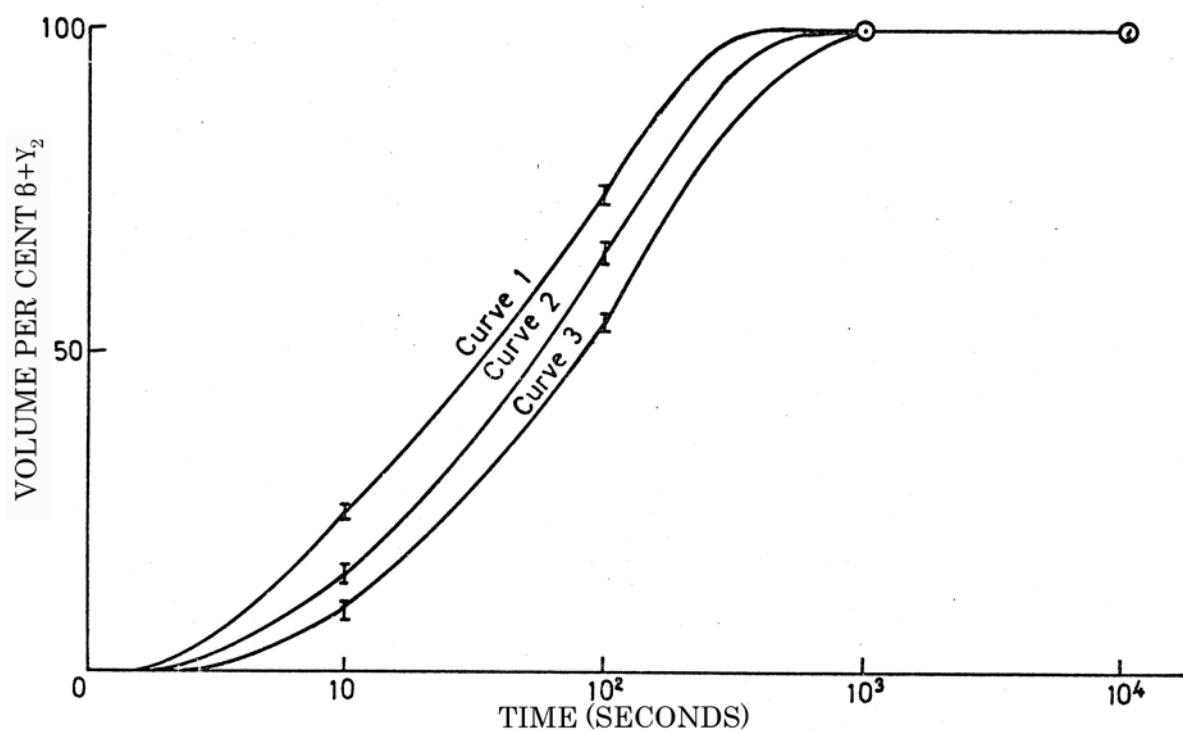


Fig. 17

Curve 1 Alloy P (22 at % Al 3 at % Sn) 848K
Curve 2 Alloy L (23 at % Al 2 at % Sn) 843K
Curve 3 Alloy G (24 at % Al 1 at % Sn) 800K

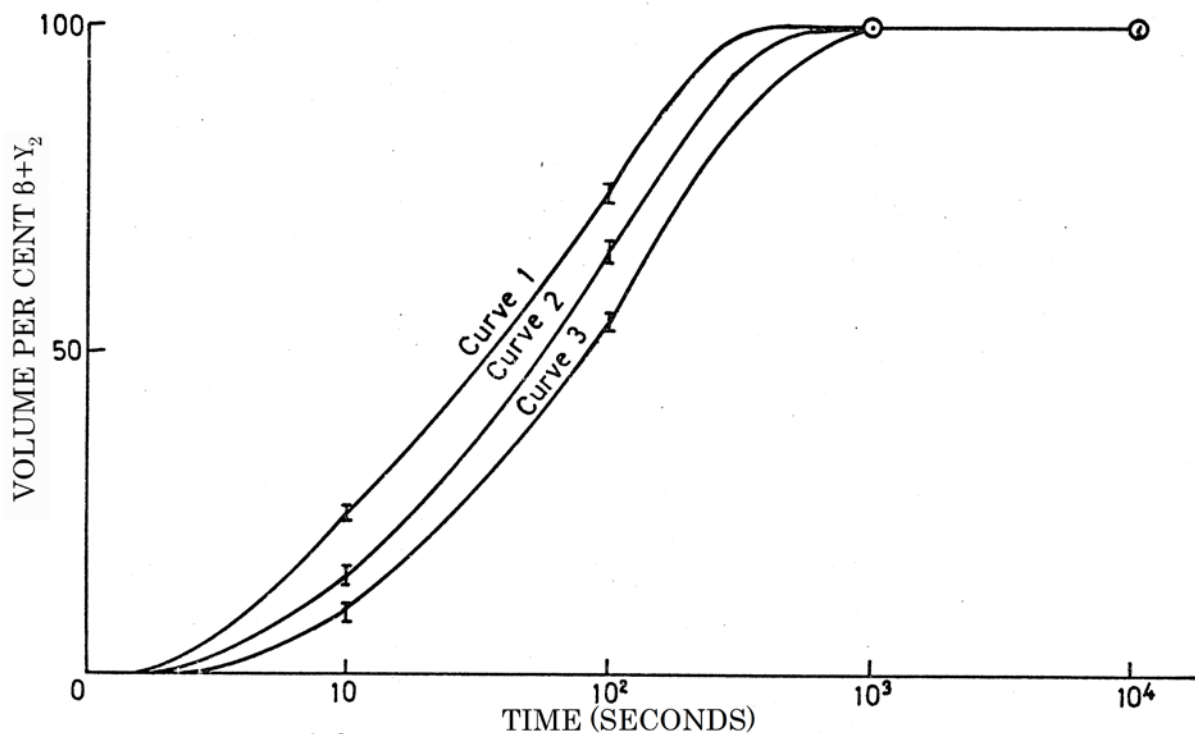
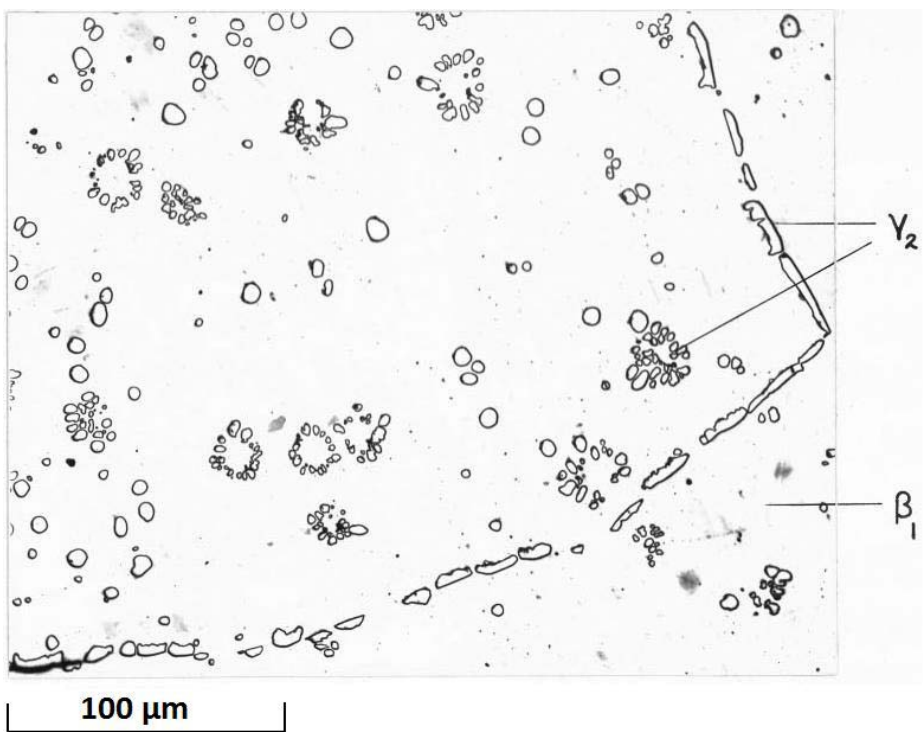
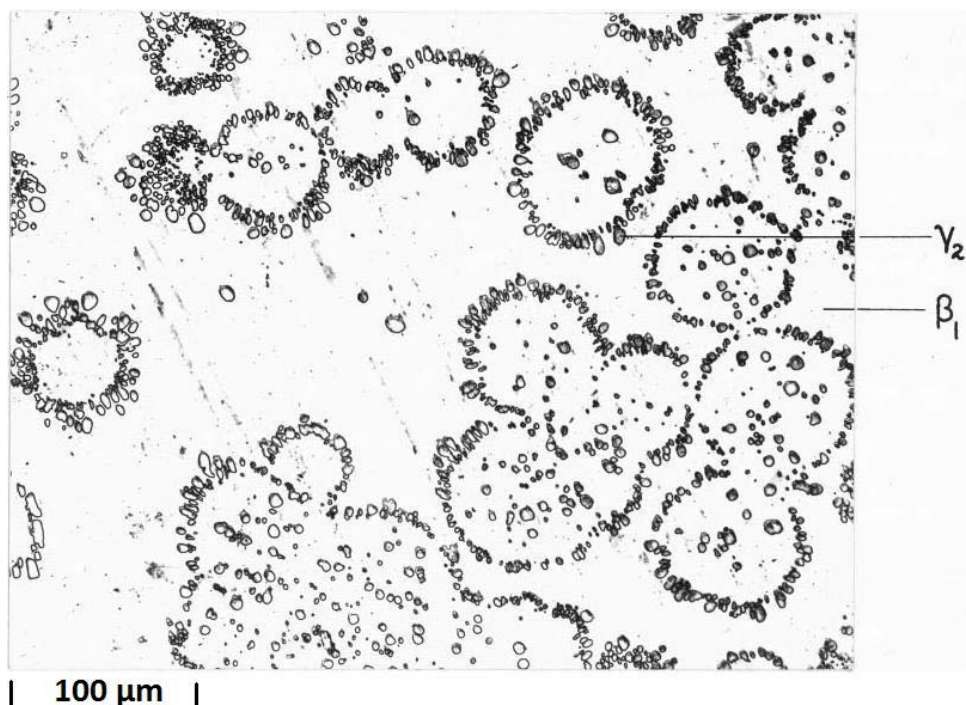


Fig. 18



(a)



(b)

Fig. 19

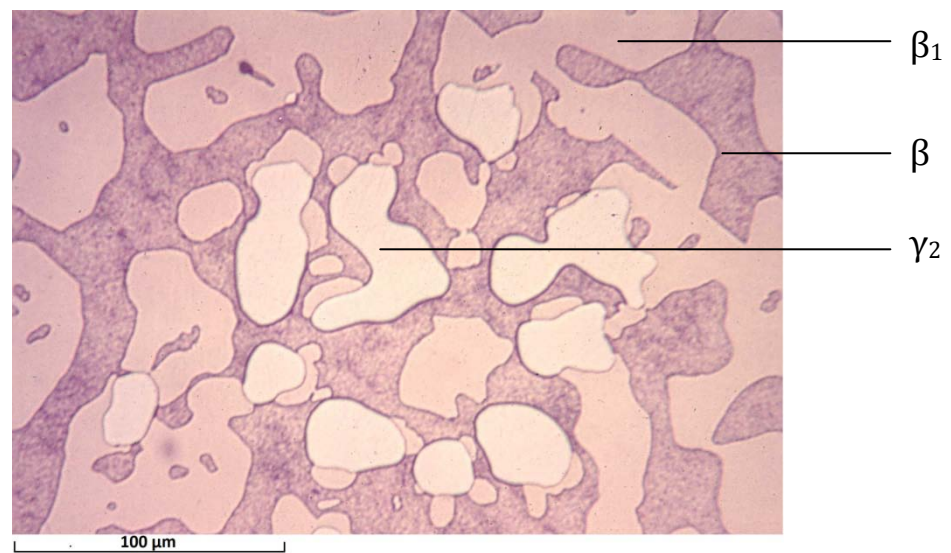


Fig. 20

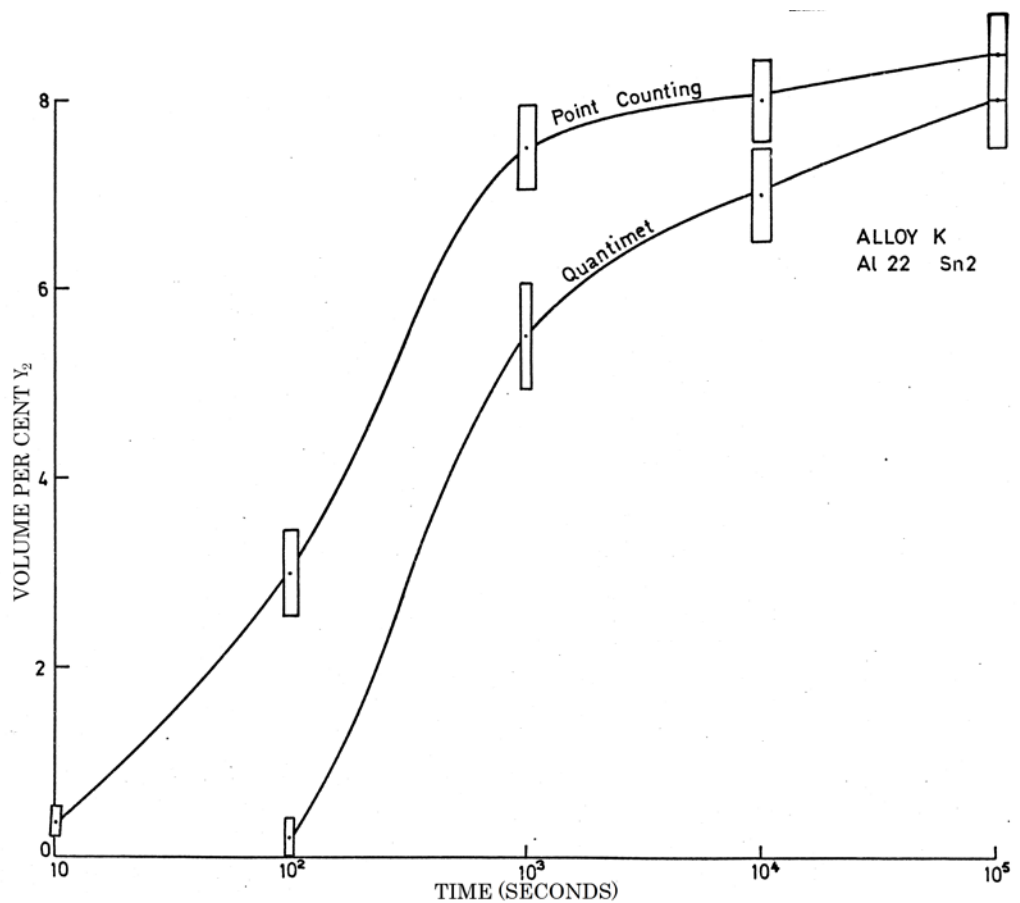


Fig. 21

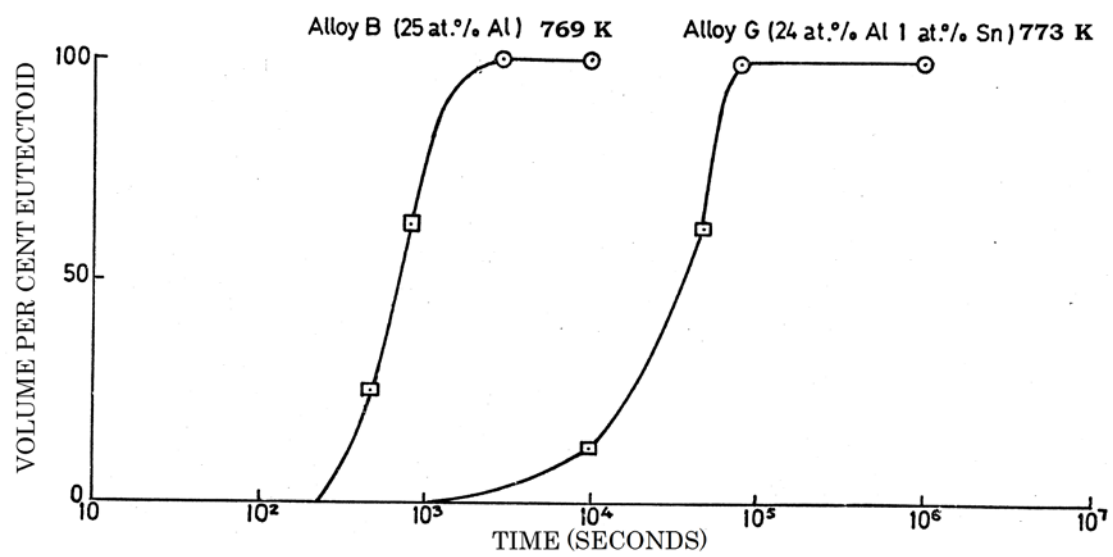


Fig. 22